https://doi.org/10.1016/j.jcsr.2022.107391

Experimental evaluation and component model for single anchored blind-bolted concrete filled tube connections under direct tension

Partha Pratim Debnath and Tak-Ming Chan*

Department of Civil and Environmental Engineering
The Hong Kong Polytechnic University, Kowloon, Hong Kong SAR, China
*Corresponding author: tak-ming.chan@polyu.edu.hk

Abstract

This paper presents an experimental programme of single anchored blind-bolted concrete filled square steel tube connections under tension to understand the joint behaviour, with emphasis on combined failure mode. A total of eight full-scale specimens were fabricated and tested. Parameters including infill concrete, length and diameter of anchored blind-bolt, tube wall thickness and concrete strength were considered. The experimental programme is accompanied by bolt preload tests and a range of material tests for all the elements in the connection. Primarily, three failure modes of the connection were identified, viz., tube wall deformation, bolt fracture and combined failure. It was observed that, apart from the beneficial effect of bolt anchorage length in enhancing the connection performance, the combined failure mode may be preferred over other failure modes for higher ductility and collapse prevention. Concrete strength is identified as the primary influential factor determining the failure modes. A component model based on spring theory is developed for prediction of global force-deformation behaviour of the bolted connection. Based on this analytical model, the strength and stiffness of such a complex connection can be predicted with good accuracy.

Keywords: Bolted connection, concrete-filled tubes, tensile load, component model, composite joints

1 Introduction

The use of structural bolts for open-section beam to closed-section column connections have been popular not only due to easy fabrication that requires less skilled labour, but also due to several advantages over the conventional welded connections. As reported in existing studies that, welded connections are not only time intensive and expensive owing to requirement of skilled workers, but also influences the structural performance due to stress concentration in the heat affected zones [1]. Currently, the construction industry is undergoing an emerging trend of use in materials like high-strength steel and high-strength concrete for higher performance and optimised sections with reduced self-weight [2, 3], and similarly, the use of high-strength structural bolts for connections have also been on the rise. The recent trend of modular buildings that are rapidly gaining popularity due to faster fabrication, reduced wastages, and improved quality, have also adopted the bolted inter-module connections due to reduced site work and demountability [4, 5]. One of the applications of high-strength structural bolts like the blind-bolt is to connect an open-section steel beam to a closed-section steel column like square hollow section (SHS), or rectangular hollow section (RHS) or circular hollow section (CHS). These steel hollow sections have their own advantages like structural efficiency and aesthetic appeal, and when they are filled with concrete, the structural performance multiplies. The prominent advantage of concrete filled steel columns is that the steel tube provides the confinement to the concrete core, and in turn the tube buckling is delayed due to presence of concrete, and thereby enhances the strength and ductility of the column [6-8]. Now, to connect these hollow steel sections, with or without infilled concrete, with open-section steel beams, the commercially available blind-bolts like the Lindapter hollo-bolt [9] and Ajax Australia bolts [10] have widely been used. But these bolted connections though provide sufficient shear and tying resistances to ensure structural safety, but have displayed low moment resisting capacities [11], and are generally regarded as pinned connections. Apart from this, the bolted connections also face slippage of bolts and severe column surface deformation. Therefore, to fully utilise the advantages of blind-bolted connections and concrete-filled steel tube columns and to explore the development of a moment-resisting bolted connection, researchers have proposed modifications in the blind-bolts.

The Ajax Australia blind-bolt was modified with an elongated shank and a headed nut, to be anchored into the concrete core of the concrete-filled hollow steel column, was proposed by Agheshlui et al. [12], and named as headed anchored blind-bolt (HABB). Later, Oktavianus et al. and Agheshlui et al. [13, 14] carried out further investigation on this modified Ajax bolt and observed enhanced strength and stiffness as compared to the standard blind-bolt. The other type of blind-bolt, called the hollo-bolt, manufactured by Lindapter International (UK) was modified with an extended shank length and headed circular nut, and called it extended hollo-bolt (EHB) by Tizani et al. [15] and Pitrakkos et al.[16]. The EHB also displayed improved stiffness characteristics due to the mechanical anchorage into the concrete, as compared to the standard hollo-bolt. The anchored hollo-bolted connection with concrete filled steel tubular (CFST) column has also been investigated under predominant shear loading by Debnath et al. [17], and observed the enhanced concrete contribution in shear load transfer. Though both the HABB and EHB have been able to improve the connection performance in terms of strength and stiffness, their installation and load transfer mechanism is distinct. Further investigation was carried out by Tizani et al. [18, 19] using the EHB to understand its potential to be used in moment-resisting connections, and two prominent failure modes can be identified: bolt failure and steel column-face failure. The bolt component failure in tension has been investigated by Pitrakkos et al.,[16] with varying parameters like bolt embedment length, bolt grade, bolt diameter and concrete strength. Whereas, for the steel column-face component failure, experimental and numerical investigations have been carried out by Tizani et al. [19], considering varied concrete strength, self-compacting and light-weight concrete. But in an actual site condition, only bolt component failure or column-face component failure would rarely arise, rather, a combined component failure mode would be generated in the EHB connection. The combined failure mode is referred to a failure of two or more components in the connection assembly. As far as combined failure mode is concerned, there has been numerical and analytical investigation by Debnath et al. and Cabrera et al. [20-22], and no independent experimental investigation is found. It is also to be stated that, in the existing finding [16], it was concluded that strength, stiffness and ductility is not influenced by bolt embedment length, and in the study [19] the influence of bolt embedment was not included, but the bolt embedment length could possibly influence the combined failure mode, and needs to be further investigated. Therefore, this experimental research programme would highlight the combined failure mode and present the influence of several component strength parameters influencing the blind-bolted concrete-filled SHS connection behaviour. It is also worth mentioning that, in a purely group bolted CFST and open-beam connection, where the beam undergoing moment forces, the bolts in the first row of the connection will experience tensile forces and the remaining will experience compressive forces. At this stage it is therefore pertinent to understand the tensile behaviour of the anchored hollo-bolted connections for combined failure modes. This experimental programme is conducted to investigate the single-bolted connection behaviour, with influence of concrete infill, EHB anchorage length, EHB diameter, concrete strength and steel tube thickness, and the observed failure modes and test findings are assessed here.

Along with the experimental findings, the paper presents a component model for prediction of the tension behaviour of single hollo-bolted CFST connection. The component model is based on spring assembly of individual elements which will be able to predict the strength and stiffness of such complex connection systems. The component model has been validated with the experimental counterparts from this study and few other experimental and numerical results in literature.

2 Experimental programme

2.1 Description of specimens

For the experimental programme, full-scale specimens were designed to understand the combined failure behaviour of the hollow and concrete filled SHS bolted connections under tension loading. In this experimental series, a total of eight specimens were fabricated, out of which two specimens can be considered as the control specimens. The square hollow steel tube specimens made of S355 hot-rolled steel are adopted for this testing programme. A cross-section size of 250 × 250 mm is considered with varied thickness of 6 mm and 8 mm, which is also a typical dimension in an actual site condition. To overcome the effect of end conditions, the length of all the specimens were originally of 1500 mm, which is sufficient to clamp with the strong floor and have an effective length of 845 mm, that does not influence the connection global behaviour. One hollow steel tube specimen without infill concrete was considered to understand the influence of concrete and tube face deformation under tensile load, and the remaining seven specimens were filled with concrete. For fabricating the blind-bolted connection circular hole was drilled will allowable clearance at the centre of the specimen. The geometric details of the specimens used are presented in Table 1. In this experimental programme, the influence of several parameters like infill concrete, bolt embedment length with anchorage, concrete grade, steel tube thickness and bolt diameter were considered, for which the detailed tabulation is made in Table 2. The nomenclature of the specimens is presented as 1-2-3-4-5, where the 1st element represents the series name, 2nd element refers to bolt diameter, 3rd element refers to bolt anchorage length, 4th element refers to grade of concrete mix, and the 5th element refers to steel tube thickness. For example, specimen A-M20-E90-C45-T6 refers series A, having bolt diameter of 20 mm with anchorage length 90 mm, infilled with concrete grade C45 and steel tube of thickness 6 mm. For determining the bolt anchorage length, the nut length can be deducted from the bolt embedment length. As the primary objective of this programme is to understand the strength and stiffness of anchored blind-bolts with varied parameters in the column, therefore the blind-bolts are fabricated via a rigid plate of 40 mm thickness, and thus the influence of beam end-plate thickness is not considered as observed in a typical beam-column connection. The blind-bolts were fixed with a wrench and applied with the required torque, which was checked using a handheld torque wrench, which ensured no over torque is applied to the bolts. The internal view of the steel tube specimens with bolt positioning and varied embedment lengths are presented in Fig. 1.

2.2 Experimental setup and procedure

The full-scale experimental investigation was carried out at the Structural Engineering Research Laboratory of The Hong Kong Polytechnic University. A 100-tons loading capacity frame, mounted on strong floor was used to conduct the tests. The specimen was rested on the strong floor and clamped in two sides with the help of 45 mm diameters strands and high-strength steel clamping plates. The single blind-bolted connection to the specimen was made via a rigid plate of 230 × 230 × 40 mm, having four holes, that provisions to connect to another rigid plate of 40 mm thickness, with the help of M30 bolts of grade 10.9. This makes the "test rig" which is attached with a 50 mm diameter shaft, that runs vertically via the loading frame beam, hydraulic jack, load cell and support plates. The hollow hydraulic jack and the hollow load cell are mounted on the beam, where the previous is connected to a hand-pump to apply the load, thus making the experiment a load-controlled based setup. As the piston in the hydraulic jack moves upward, it also simultaneously pulls the test rig, which eventually applies direct tensile pull-out force to the blind-bolted connection, and the load cell sensor detects the load-displacement and is recorded using the data-logger. It is worth mentioning that, at the beginning of every test, a preload of 10 kN was applied to check the instrumentation employed, and the original test would start after the release of this preload. Fig. 2 (a) shows the schematic 2-dimensional representation of the test set up, and Fig. 2 (b) presents the 3-dimensional view of the experimental setup. The clear distance between the two clamps can be considered as the effective length of the specimen, which is around 845 mm, which can be seen in the close-up view of the test setup as presented in Fig. 3.

2.3 Instrumentation

The deformation and the strain measurements at points of interest were measured with the help of linear variable differential transducers (LVDTs) and strain gauges. A total of eight LVDTs were used in the experimental investigation, where two LVDTs (L1 and L2) were mounted on the rigid plate via which the blind-bolted is connected to the specimen, which would measure the bolt head displacement, or the global connection behaviour. Two LVDTs (L3 and L4) were placed close to the connection plate (around 5 mm away from the plate) to measure the tube wall deformation, and two transducers (L5 and L6) were used to measure the deformation at the centre of the vertical walls of the column specimen. To keep check of any uplift of the specimen, two LVDTs (L7 and L8) were mounted at the centre of the clamps, which can later be used to measure the actual displacement of the connection. Several strain gauges were attached to the specimen to understand the influence of different parameters on the hollow and concrete filled SHS column. Two strain gauges (SG1 and SG2) were fixed on the tube wall near to the connection plate (around 10 mm away from the plate) to measure the strain development in the region. Though fixing strain gauges on the tube wall near the bolt hole would be more appropriate to understand the tube wall yielding phenomenon, but as the rigid plate is bolted to the steel tube using high amount of torque, this could damage the strain gauge. Two additional strain gauges (SG3 and SG4) were fixed at around 200 mm away from the connection plate (i.e., around 315 mm away from the bolt hole centre), to observe the influence of several parameters at this location. As under the direct tensile load applied at the connection, the vertical walls of the column specimen will also be under either compressive or tensile stresses, two strain gauges (SG5 and SG6) were fixed at the centre of the vertical walls of the tube. To understand the contribution of the extended bolt shank embedded into the concrete core, a strain gauge (SG7) was fixed immediately next to the nut attached to the bolt shank. For fixing this strain gauge, the bolt thread was flattened to a certain length, without reducing the core tensile area of the bolt. The positioning of the LVDTs and the strain gauges are presented in Fig. 4. It is worth mentioning that strain gauge was not fixed to the standard blind-bolts due to insufficient length, and assuming little contribution from connections without any anchorage element. The parts of an extended blind-bolt along with the location of attached strain gauge is shown in Fig. 5.

2.4 Material tests and properties

In this experimental programme, material tests for the blind-bolt shank, bolt sleeves, steel tube and concrete were carried out. To determine the material properties of the SHS steel tubes, both flat and corner coupons were extracted from steel tubes of the same batch as used in the experiment. Also, for the blind-bolts, circular coupons were prepared for all the batches of bolts, having different shank length and diameters. The sets of steel flat coupons, curved coupons, and bolt circular coupons were designed as per ISO 6892-1:2019(EN) [23], and tests were conducted using the Instron 8803 servo-hydraulic system. In this experimental programme, steel tubes of 6 mm and 8 mm were used, and for blind-bolts, bolt shank length of 120 mm, 150 mm, and 165 mm were used, each of them supplied from different batches. For the steel tube flat coupons and bolt circular coupons, three specimens of each type were prepared, and the average of yield strength, ultimate strength and elastic modulus is reported. Whereas, for steel tube curved coupons, two coupons were prepared for each batch of steel tube. The curved coupons were extracted from diagonally opposite corners of the square hollow steel tubes and the average yield strength, ultimate strength and elastic modulus is reported. For the steel tube coupons, a loading rate of 0.3 mm/min until 3% strain, and 0.6 mm/min from 3% strain to yield strain was used, whereas, for bolt circular coupons 0.02 mm/min was adopted until 1% strain, and 0.2 mm/min loading rate was used from 1% strain to 7% strain. Beyond the yield strain a higher loading rate was used until necking of the coupons. The setup used for the circular coupons is presented in Fig. 6, and the representative samples of the tested steel coupons are shown in Fig. 7. As the bolt expandable sleeves forms an important part of the blind-bolt connection system, hardness test was conducted to estimate the yield strength and ultimate strength of the sleeve component. Since the expandable sleeve is hollow, its leaves were separated, and then was used to measure the strength properties with the Rockwell hardness testing machine and can be referred from Fig. 8.

The stress-strain plots for the steel tube of 6 mm thickness are presented in Fig. 9 for reference. As the steel tube having 6 mm thickness was fabricated by welding two channel sections, therefore the coupons for weld regions were also prepared and investigated for the mechanical properties. The stress-strain curves for the bolt coupons are presented in Fig. 10. The measured mechanical properties for the bolt, sleeve and steel tube are presented in Table 3. The chemical composition as per the mill certificates for the blind-bolts used in this experimental programme is also presented in Table 4.

Three different grades of concrete were used as infill for the hollow steel tubes, and therefore the concrete cylinders were prepared to determine the compressive strength and split tensile strength. At least three cylinders were used to determine concrete material properties, where the elastic modulus was based on the strain gauge readings that were fixed on the cylinders. The stress-strain graph of all the three grades of concrete is presented in Fig. 11, whereas the mix design and obtained material properties are presented in Table 5.

2.5. Bolt preload test

As this experimental programme involves bolts with application of preload, a separate setup was also prepared to measure the preload induced in the blind-bolts and observe its relaxation over a period. Previously, experimental and numerical investigation on bolt preload relaxation for extended hollo-bolted CFST connection was conducted by Cabrera et al. [24], and observed that most preload losses occur from 2 h for standard hollo-bolts to 24 h for extended hollo-bolts. In the current experimental programme, further tests are carried out to obtain the residual preload for hollo-bolts of different grade as this can influence the connection global behaviour and, needs to be considered for conducting accurate numerical analysis. Three M20 blind-bolts of different grades and lengths was considered for this test, and the required tightening torque was applied. To measure the applied bolt preload or the clamping force, a 220 kN capacity thru hole load cell was employed. The load cell was placed or sandwiched between the blind-bolt collar and a rigid plate of 40 mm thickness, that was used to resemble same clamping thickness as in the experimental setup of tensile pull-out testing series. The load cell was connected to a data logger to record the load applied. The arrangement for the measurement of blind-bolt preload is presented in Fig. 12. After applying the bolt preload with the handheld toque wrench, the load relaxation was observed for about 70 h (approximately 3 days), which is presented in Fig. 13. As observed from Fig. 13, the preload drops sharply in the initial three hours for all the bolts and then, drops gradually until 36 h for M20 bolts of grade 10.9, and 48 h for M20 bolts of grade 8.8. The preload measurement is presented in Table 6, which shows that about 76% and 91% of applied initial preload is residual preload after 48 hours of relaxation for M20 bolts of grade 8.8 and 10.9, respectively.

3 General observation and failure modes

The physical damages observed during the experimental programme and the failure modes of all the specimens are presented here. The specimen A-M20-E0-C0-T8 is a hollow tube, without any infill concrete, and the standard hollo-bolt was used to fabricate the connection. As the tensile load is applied to the connection, the load is transferred to the hollow tube column by the expandable sleeve bearing on the tube wall. The expandable sleeves are supported by the conical nut fitted on the bolt shank. The initial deformation of the specimen is by flexible deformation of the column face, and inward deformation of the vertical side walls. As the loading is further applied, the expandable sleeves reach its ultimate strength and approaches towards rupture of the sleeve leaves. This rupture can also be seen progressing along the slit line of the sleeve. Therefore, the stages of failure are the tube wall face deformation, followed by bolt sleeve fracture, and no damage in the bolt shank, as presented in Fig. 14. For specimen A-M20-E0-C45-T8, the standard hollo-bolt was used to fabricate the connection, and the steel tube had concrete infill. There is a bolt embedment of 65 mm (refer Fig. 1), but as there is no headed nut attached to the shank, there is technically no anchorage element into the concrete core. Under the applied tensile forces, the flexible deformation of column face is observed, and with continued loading, the conical nut of the bolt comes out from the tube hole, along with fractured sleeve. The tube deformation around the bolt and sleeve fracture can be seen from Fig. 15 (a).

The specimen A-M20-E75-C45-T8 was fabricated with an anchorage of 75 mm, the concrete filled SHS specimen is observed to have delayed tube wall deformation. The initial failure stage is concrete crushing, which is followed by tube wall deformation around the bolt hole. For safety during the experiment, it was initially decided to stop applying further load after a drop of around 20% of peak load value. Therefore, for this test specimen which involved the anchorage bolt, the load application was stopped after the load dropped to 150 kN. But soon after inspection by removal of the steel tube skin, it was found that there is no necking of bolt shank, and further loading to the connection can be applied for the following test specimens to monitor the ductile behaviour. The deformation of the connection for the specimen A-M20-E75-C45-T8 can be seen in Fig. 15 (b), and the concrete crushing damage is presented in Fig. 16 (a), after removal of the steel tube wall in the connection region. The specimen A-M20-E90-C45-T8 had an elongated bolt anchorage length of 90 mm, at the initial stages of the experiment, there is limited deformation in the tube, but with continued loading, the tube wall deformation around the bolt hole can be observed. With further loading, the bolt sleeve appears to have cracks, and coming out from the tube hole along with the bolt conical nut. Parts of concrete can also be seen coming out though the sleeve slit regions, which confirms the concrete crushing inside the column tube. The images of concrete crushing, tube wall deformation and bolt sleeve fracture are presented in Fig. 16 (b).

To investigate the influence of concrete grade, specimens with three grades of concrete C25/30, C45/55 and C80/95 were tested. As the normal concrete grade of C45/55 is usually used in hollow steel tubes as infill concrete, this grade of concrete is considered as the standard grade. Also, as in the recent decades the use of high-strength materials has gained popularity, the use of C80/95 is also considered in this experiment to understand the influence of higher concrete grade in connection behaviour. C25/30 is another normal strength concrete used in construction and is also used as an infill to realise its influence on the global connection behaviour. The specimen A-M20-E90-C25-T8 with a reduced concrete strength of 26 MPa failed in a similar mode as that of A-M20-E90-C45-T8, where concrete crushing is followed by deformation in the steel tube around the bolt hole, and then fracture in the bolt sleeve. But due to the reduced concrete strength, the concrete crushing is severe, and the damage is evident over a larger area. As far as the bolt shank is concerned, no necking is observed. The combined failure mode of this specimen is presented in Fig. 17 (a). For the specimen A-M20-E90-C80-T8 with a higher strength concrete of 82 MPa, the failure mode is dominated by bolt shank necking and very limited damage in the concrete and tube wall. Unlike previous specimens, there is no visible damage in the bolt sleeve, which also indicates that most of the loading was borne by bolt anchorage mechanism and thus leading to shank necking and fracture. There is also insignificant tube wall deformation around the bolt hole. The concrete surface and the failed bolt shank is presented in Fig. 17 (b) for reference.

The specimen A-M20-E90-C45-T6 was tested to understand the influence of tube thickness, where tube of 6 mm was used. With reduced tube wall thickness, initially has concrete crushing and then followed by tube wall yielding. With continued loading, the tube wall deformation is more evident, and gradual pull out of the bolt sleeve. In this test, there is no necking of bolt shank and global connection behaviour is mostly governed by concrete damage and column face deformation. The failed specimen is presented in Fig. 18 (a).

To investigate the influence of bolt diameter specimen A-M16-E90-C80-T8 consisted of M16 bolt, where the prominent failure mode for this specimen is necking and sudden fracture of the bolt shank. There is no visible damage in the bolt sleeve, and the deformation in the column face wall is also not prominent. It is worth mentioning that the location of the bolt shank fracture is in the region between conical nut and bolt head; and not between conical nut and the hexagonal nut embedded in the concrete core. The failure mode and the location of bolt fracture is similar to the specimen A-M20-E90-C80-T8. The image of the failed specimen is presented in Fig. 18 (b).

4 Test results and discussion

4.1 Load-deformation behaviour

The global load-displacement behaviour of the single-bolted connections with hollow and concrete filled SHS columns are plotted by taking the average of LVDT1 and LVDT2. To better analyse the overall behaviour of the connections with due consideration to initial stiffness, strength, ductility and failure mechanism, the plots are illustrated in groups with comparable parametric changes. For the specimen A-M20-E0-C0-T8, the connection displays an elastic behaviour with an initial stiffness of 32 kN/mm and starts yielding at 43 kN. The initial stiffness is contributed by the column tube wall, and as the loading is further applied, the tube wall starts deforming where the load is transferred to the column face by sleeve bearing. The ultimate capacity of the connection is reached at around 110 kN, and then there is a gradual drop in the connection strength due to fracture in the sleeve. A significant increase in stiffness can be observed in the specimen A-M20-E0-C45-T8 due to presence of infill concrete. As the concrete present inside the SHS column prevents the inward deformation of the vertical side walls of the tube, additional strength is developed from the corner region, which thereby enhances the strength and capacity of the connection. The connection begins to yield at around 48 kN, which is close to the previous specimen A-M20-E0-C0-T8, but the initial stiffness jumped to around 90 kN/mm. Beyond 48 kN, the slope of the load-displacement curve does not run rapid, and still possess enough strength possibly due to the presence of concrete which stiffens the expanded sleeves. After a deformation of 7 mm, the tube wall starts yielding, and gradually reaches the ultimate load of 123 kN, and fails by sleeve fracture upon further loading. The comparative plot of A-M20-E0-C0-T8 and A-M20-E0-C45-T8 is presented in Fig. 19 (a), where the stiffness and strength enhancement can be visualised.

The influence of headed anchored elongated bolt shank and the anchorage length are the key parameters of this investigation. For the specimen A-M20-E75-C45-T8, where an anchorage length of 75 mm was made into the concrete core, a significant improvement in the connection strength and stiffness is observed as compared to the specimen A-M20-E0-C45-T8, where no anchorage element was present. In Fig. 19 (b), it can be observed that the connection A-M20-E75-C45-T8 displays a stiff behaviour, which can be ascribed to the load transfer to the concrete core by the bolt anchorage. As the loading is continued, the concrete tensile cracks start developing, and leads to crushing, as a result of which a sharp load drop is obtained in the plot. With further application of load, the forces are now transmitted to the column tube wall by bolt sleeve bearing, and thus there is again a gradual increase in load-displacement behaviour until the bolt sleeve fractures. A similar trend can be observed for A-M20-E90-C45-T8, where a longer bolt anchorage of 90 mm was used, and a higher strength was achieved. Though the initial stiffness of A-M20-E75-C45-T8 and A-M20-E90-C45-T8 are very close at the beginning, but beyond 90 kN there is a slight drop in the stiffness for the specimen with 90 mm anchorage, possibly due to some air gaps present in the concrete, arising due to compaction issues. The connection capacity drops significantly after the tube wall yielding and followed by failure of the sleeves. Strength achieved by the connections A-M20-E75-C45-T8 and A-M20-E90-C45-T8 are 170 kN and 185 kN, respectively, which is a significant improvement of about 38% and 50% as compared to A-M20-E0-C45-T8.

The influence of infill concrete strength on the connection behaviour is presented in Fig. 19 (c). The specimen A-M20-E90-C25-T8 having concrete infill of cylinder strength 26 MPa presents a reduced connection stiffness as compared to A-M20-E90-C45-T8, which can be attributed to lesser concrete tensile and compressive capacity and leading to early concrete crushing. But the stages and sequence of failure remains to be concrete crushing, followed by tube wall yielding and sleeve fracture. When a higher concrete grade was used in A-M20-E90-C80-T8, there has been an increase in the connection stiffness owing to the higher elastic modulus of concrete, but the failure mode is dominated by bolt shank failure. Due to improved concrete component, the bolt shank became the weaker component, and thus little to no concrete cracking was observed, and the connection failed by shank necking and ultimately by fracture. Though this connection achieved a higher strength of 197 kN (which is very close to the bolt ultimate capacity), this failure mode cannot be regarded as a combined failure mode.

The comparison for concrete filled SHS column with higher *b/t* ratio is presented in Fig. 19 (d), where specimen A-M20-E90-C45-T6 exhibits lower connection strength, due to lesser tube wall contribution as compared to its counterpart specimen with 8 mm tube thickness. Also, the tube deformation is higher and starts to yield at the lower load of 159 kN, which is 16% less than A-M20-E90-C45-T8. It is to be noted that, the stiffness of connection A-M20-E90-C45-T6 did not display much stiffness degradation as expected, as this steel tube was fabricated by welding two channel sections, and thus have weld seams on two sides of the tube, thereby enhancing the stiffness property of the connection. The influence of bolt diameter in extended blind-bolted connection is presented in Fig. 19(e), which shows that the connection A-M16-E90-C45-T8 failed by bolt fracture at a load of 144 kN, which is also close to the ultimate load capacity (142 kN) of the M16 bolt. In this connection, even with a normal concrete grade of 46 MPa, the reduced bolt diameter of 16 mm forms the weakest element, and thereby leading to bolt necking and fracture.

The measured connection strength, connection stiffness at 50% bolt capacity, deformation at peak load, and observed failure modes are presented in Table 7. In an actual practical site condition, the bolts would be expected to be the strongest element in the connection assembly, and therefore the stiffness is measured at 50% of bolt ultimate capacity for having an appropriate comparable feature between the specimens. Apart from the above discussion, the beneficial effect of adding concrete in hollow tube and providing anchorage element in the concrete core also led to significant reduction in column vertical wall which was measured using LVDT6.

4.2 Strain response in steel tube wall

To accurately observe the deformation behaviour and the stress level in the steel SHS, several strain gauges were attached on the tube surface. The arrangement of the strain gauges was illustrated in Fig. 4. The positive strain implies tension, and the negative strain implies compression. SG1 and SG2 measured the tube strains at the location close to the connection plate, and the plots are shown in Fig. 20. The tube strain for the concrete un-filled hollow specimen A-M20-E0-C0-T8 reached a maximum strain of -1200 $\mu\varepsilon$, whereas for the concrete filled specimen A-M20-E0-C45-T8, the maximum strain reached almost -2000 $\mu\varepsilon$, signifying enhanced tube wall contribution in connection strength. As the load application after load drop of 150 kN was stopped, the strain measurement for the specimen A-M20-E75-C45-T8 could not be fully realised, but for the specimen A-M20-E90-C45-T8 the tube strain could reach the steel yield strain of -2400 με signifying the full yielding of the tube wall. A similar trend can also be observed for the specimen A-M20-E90-C25-T8. But for the specimen A-M20-E90-C80-T8, as most of the connection strength was contributed by bolt anchorage mechanism and carried by the bolt shank, there is very limited strain development in the steel tube, and a similar reason can be attributed for the specimen A-M16-E90-C45-T8.

SG3 and SG4 are the strain gauges attached at mid-surface between the connection plate and clamping plates of the specimens. The strain measurement of these location is represented in Fig. 21. Except the specimen A-M20-E0-C0-T8 which shows negative strain, all the other specimens display positive strain unlike the SG1 and SG2 readings. It signifies that for the concrete un-filled specimen, the part of the steel tube beyond connection region was under compressive stresses. Whereas, for the remaining concrete filled specimens, positive strain was recorded, signifying the stresses at this location have undergone tensile forces due to the underlying support of concrete.

4.3 Strain development in anchored bolt

To ascertain the contribution of bolt anchorage into the concrete core, the strain gauge SG7 was used to record the strain generated in the bolt shank. The measured strains are shown in Fig. 22, where six out of eight specimens containing elongated shank and headed nut were considered. For the specimen A-M20-E75-C45-T8, the maximum amount of positive strain (tensile) developed at the bolt shank near the headed nut is about 2100 με, whereas, for the specimen A-M20-E90-C45-T8 the strain developed is about 3200 με, which signifies higher load transfer into the concrete core due to larger bolt anchorage length. In the case of A-M20-E90-C25-T8, due to lower concrete strength and early concrete damage, the strain developed in the anchored bolt was limited to about 2000 με. Though for the specimen A-M20-E90-C80-T8, the strain generated in the bolt shank near the nut end did not reach the bolt yield strain value, but from the previous discussion it was observed that the bolt had fractured at the location between the conical nut and bolt head. This signifies that there was more stress developed between the conical nut and bolt head, as compared to the location between conical nut and concrete embedded headed nut. The bolt strain value of about 3150 $\mu\varepsilon$ developed in the specimen A-M20-E90-C45-T6 also indicates significant contribution of anchorage element for enhanced composite action in the connection. For the specimen A-M16-E90-C45-T8, the strain developed is very close to the bolt yield strain, which confirms that bolt necking and fracture in the shank location between conical nut and bolt head. The plots in Fig. 22 also presents the strain development with respect to the concrete strain at its peak stress, signifying initiation of concrete damage for those crossing the concrete strain at peak stress limit.

5 Component model development

To estimate the hollo-bolted connection strength and stiffness, an analytical approach is presented based on the individual component spring model. The tensile behaviour of such a connection depends on the individual performance of the tube wall, hollo bolt shank, bolt head anchored in concrete, and the bolt expandable sleeve. The strength arising from bond between the embedded threaded shank and the adjoining concrete is ignored, as the strength enhancement is insignificant as observed by Debnath et al. [20]. In this section, the tensile behaviour of each connection component has been presented as a massless spring model, and when assembled will be able to give a fair representation of the overall connection behaviour. In the blind-bolted CFST connection, the anchorage component, embedded bolt component and the sleeve are connected end-to -end, forming a single path of load transmission, therefore these components can be arranged in series configuration. Secondly, the above arrangement is connected to the tube wall across each other, and thus can be considered a parallel configuration. Again, this entire arrangement is connected end-to-end with the free bolt, and hence, this can be considered in a series. The connection components are shown in Fig. 23 (a) and the assembly of spring is shown in Fig. 23 (b). The spring assembly is arranged based on experimental observations discussed in the previous sections. From current experimental observations and previously conducted numerical investigations [20], it may be simplified and stated that, at the initial stage the load is borne by the concrete anchorage, embedded bolt and the sleeve, which is then gradually transferred to tube after concrete failure, and then pulled out by the free bolt part (necking of shank). Thus, the concrete anchorage, embedded bolt and the expandable sleeve are in series, which together are arranged in parallel with tube wall, and again is in series with the free bolt. Here, the free bolt refers to the standard hollo bolt shank length, and embedded bolt is referred to the extended shank length. To combine the components as per the spring theory, the following basic equations apply:

Series configuration:

$$k = 1/\left(\frac{1}{k_1} + \frac{1}{k_2}\right) \tag{1}$$

$$F = min(F_1; F_2) \tag{2}$$

Parallel configuration:

$$k = k_3 + k_4 \tag{3}$$

$$F = F_3 + F_4 \tag{4}$$

$$\delta = min\ (\delta_3\ ; \delta_4) \tag{5}$$

5.1. Hollo bolt shank in tension component

The tensile behaviour of the hollo bolt is modelled based on the bolt coupon tests and general strength and stiffness formulation. The free bolt part and embedded bolt part are modelled separately for higher accuracy of the assembled component model as shown by Oktavianus et al. [25] for anchored Ajax bolts. The equations for yield ($F_{y,b}$) and ultimate strength ($F_{u,b}$) for the hollo bolt is presented in Eqs. (6) and (7):

$$F_{y,b} = A_b f_{y,b} \tag{6}$$

$$F_{u,b} = A_b f_{u,b} \tag{7}$$

where, A_b is the hollo bolt tensile area, $f_{y,b}$ and $f_{u,b}$ are the yield and ultimate tensile strength of the hollo bolt shank material.

The initial ($K_{1,b}$) and the second stiffness $\left(K_{2,b}\right)$ of the bolt shank can be determined from the following equations:

$$K_{1,b} = \frac{A_b E_b}{l_b} \tag{8}$$

$$K_{2,b} = 0.08 K_{1,b} \tag{9}$$

Where, $E_b$is the Young's modulus of the bolt shank, and l_b is the length of the bolt shank. For the free hollo bolt shank, l_b is calculated by summation of thickness of bolt collar (t_{bc}), end plate (t_{ep}) (here rigid plate), thickness of column tube wall (t_{tw}) and length of the bolt conical nut (l_{cn}). Whereas, for embedded bolt, l_b is calculated by deducting the free bolt length from the total bolt shank length (please refer Fig. 23a).

5.2. Hollo bolt expandable sleeve component

As the expandable sleeves transfers the force by bearing in a pull-out loading, it is therefore important to consider the influence of sleeve component. From experimental investigations in this paper and numerical simulations conducted by Debnath et al. [21] it was observed that hollo bolted connections can fail by sleeve fracture when subjected to tensile loading, and was also influenced by the infill concrete that stiffened the sleeve leaves. As presented in this paper, hardness tests were conducted for the sleeve material, and its yield and ultimate strengths were computed. For defining the behaviour of expandable sleeve, the tri-linear idealised force-slip model by Pitrakkos et al. [26] that considers the concrete grade and bolt class is adopted here. The ultimate strength ($F_{u,sl}$) is computed as per eq. (10)

$$F_{u,sl} = A_{sl}\, f_{u,sl} \tag{10}$$

Where, A_{sl} is the net sleeve area, and $f_{u,sl}$ is the ultimate strength of the sleeve material.

The first yield point and second yield point are presented in Eqs. (11) and (12), respectively

$$F_{y1,sl} = X . F_{u,sl} \tag{11}$$

$$F_{y2,sl} = Y . F_{u,sl} \tag{12}$$

Where, X and Y are coefficients, given as 0.25 and 0.68 respectively for M20 grade 8.8 bolts, whereas the values are 0.60 and 0.90 respectively for M16 grade 8.8 bolts.

The initial stiffness is presented as a product of normalized initial stiffness of the element (k_{norm}) and the sleeve ultimate strength, as given in eq. (13). The secondary stiffness beyond the first yield point and stiffness beyond second yield point is given by eq. (14) and (15) respectively.

$$K_{1,sl} = k_{norm}\, F_{u,sl} \tag{13}$$

$$K_{2,sl} = \mu^{p}\, K_{1,sl} \tag{14}$$

$$K_{3,sl} = \mu^{u}\, K_{1,sl} \tag{15}$$

The k_{norm} values are $1.114\ mm^{-1}$ and $1.091\ mm^{-1}$ for M20 bolts grade 8.8 and M16 bolts of grade 8.8, respectively. In eq. (14) and (15), μ^{p} and μ^{u} are the strain hardening coefficients, with values 0.298 and 0.087 respectively for M20 bolts of class 8.8, whereas 0.289 and 0.032 for M16 respectively, for M16 bolts of class 8.8.

5.3. Column tube wall in tension component

To estimate the individual tensile behaviour of column tube wall, the nominal pull-over strength of sheet per screw equation provided by the AISI S100-16 [27] is considered as a reference. The strength of the tube pull-over is stated to be a function of tube wall thickness, screw washer thickness, washer diameter, hole diameter and tube ultimate strength with a multiplier co-efficient of 1.5, along with other boundary conditions. As for hollo-bolted connections, the bolt holes are significantly large (about 1.75 times the bolt diameter), a modified co-efficient value of 0.7 is found to be appropriate for the current study. Also, for hollo bolted connection, as the tube bearing is by expandable sleeve and not washer, therefore an approximation of 2 times the bolt diameter is assumed as equivalent to washer diameter. Thus, the modified equation for ultimate tensile strength ($F_{u,tw}$) of the column wall is given by eq. (16):

$$F_{u,tw} = 0.7\, f_{u,tw}\, 2d_b\, t_{tw} \tag{16}$$

Where, $f_{u,tw}$ is the ultimate tensile strength of the steel tube material, d_b is the bolt diameter, and t_{tw} is the tube wall thickness.

As observed by [13] for tests of headed anchored Ajax bolts, the stress concentration around the bolt hole will lead to local yielding ahead of the overall tube yielding, therefore two yield points are provided. As in the current study, the hollo bolted connections were fabricated with upper limit of bolt hole (35 mm diameter hole for 32.75 mm sleeve diameter), the first yield point ($F_{y1,tw}$) is given by modified eq. (17), and second yield point ($F_{y2,tw}$) of the tube wall is presented in eq. (18):

$$F_{y1,tw} = 0.4\, F_{u,tw} \tag{17}$$

$$F_{y2,tw} = \frac{f_{y,tw}}{f_{u,tw}}\, F_{u,tw} \tag{18}$$

Where, $f_{y,tw}$ is the steel tube material yield strength.

For obtaining the stiffness of the tube wall, the equations proposed by Liu et al. [28] for steel channel face, Málaga-Chuquitaype et al. [29] for column face component, and Oktavianus et al. [25] for column tube wall with bolted connection is taken as reference, and a modified equation for square column sections having hollo-bolted connection is presented. The proposed equation has also been calibrated to capture the stiffness of the column tube wall arising from infill concrete and is presented in eq. (19). For hollow tube without concrete infill, the stiffness was significantly reduced by almost three times, and the modified eq. (20) is used to predict initial stiffness for tube without concrete.

$$K_{1,tw} = \frac{\pi E_{tw} t_{tw}^2}{4(1-\upsilon^2).B} \left(\frac{2d_b}{d_{hole}}\right)^{12} \quad (19)$$

$$K_{1,tw} = \frac{\pi E_{tw} t_{tw}^2}{12(1-\upsilon^2).B} \left(\frac{2d_b}{d_{hole}}\right)^{12} \quad (20)$$

Where, $K_{1,tw}$ is the initial tube wall stiffness, E_{tw} is the elastic modulus of tube wall, υ is the steel Poisson's ratio, B is the column width, and d_{hole} is the bolt hole diameter.

The values for secondary stiffness of the tube wall can be represented as a percentage of initial stiffness as also previously shown by Málaga-Chuquitaype et al. [29]. Similarly, in this paper the stiffness ($K_{2,tw}$) beyond the first yield point is given as 40% of the initial stiffness, and the stiffness ($K_{3,tw}$) beyond second yield point is given as 10% of the initial stiffness, as presented in eq. (21) and (22). It is observed that the selected percentage values give a good representation of the infill concrete and corner curvature of the square columns used in this testing programme.

$$K_{2,tw} = 0.4\, K_{1,tw} \quad (21)$$

$$K_{3,tw} = 0.1\, K_{1,tw} \quad (22)$$

5.4. Concrete anchorage component

As observed in the experimental failure modes in this paper, the concrete crushing followed by cone formation has been prominent for all the combined failure modes. The concrete crushing damage is initiated around the bolt anchorage nut. The American code ACI 318 [30] gives the load at which the crushing of the concrete occurs due to the bearing of the headed anchor as presented in eq. (23).

$$F_{c,conc,ACI} = 8\, A_{brg} f_c' \tag{23}$$

Where, A_{brg} is the net bearing area of the anchored head, f_c' is the characteristic compressive strength of concrete. But the above equation is limited for usage only when the net bearing area of the head is at least greater than 4 times area of the bar (here bolt). But in the current study, the diameter of the headed nuts are around 1.5 and 1.45 times the bolt diameter of M16 and M20 respectively, and thus above equation may highly overestimate the concrete crushing strength. As shown in numerical studies by Debnath et al. [20], that the current available headed nut dimension is sufficient to generate enough connection stiffness, and using a larger diameter nut does not significantly influence the connection strength, therefore a modified equation for concrete crushing strength is presented here, as given in eq. (24)

$$F_{c,conc} = 2\, A_{brg} f_c \tag{24}$$

where, f_c is the cylinder compressive strength of concrete.

The load prediction eq. (23) by ACI 318 does not refer to the strength required to completely pull out the anchor from the concrete, and therefore it does not contain any factor related to embedment depth. To determine the pull-out strength of anchor from concrete, the equation proposed by Eligehausen et al. [31] is used, as in eq. (25):

$$F_{u,conc} = 16.8 \sqrt{f_c}\, h_{eff}^{1.5} \tag{25}$$

where, h_{eff} is the bolt anchorage effective length, as shown in Fig. 23.

The concrete crushing strength ($F_{c,conc}$) and the pull-out strength ($F_{u,conc}$) can be considered as the yield and ultimate strength of the anchorage component. To determine the initial and secondary stiffness of the anchorage component, the equation proposed by Oktavianus et al. [25] for Ajax headed anchored bolts is used, which is given in Eqs. (26) and (27), respectively:

$$K_{1,conc} = \frac{\pi\, E_c d_b}{4} \tag{26}$$

$$K_{2,conc} = 0.05\, K_{1,conc} \tag{27}$$

where, E_c is the elastic modulus of concrete.

6 Comparison with test results

The component model presented in the earlier section was validated with the experimental test results as presented in section 4.1. The comparison between the load-deformation plots of the experimental and the predicted analytical models are presented in Fig. 24 (a-h). As seen from Fig. 24, the component model has a good agreement with the experimental counterparts, in terms of initial stiffness and peak load. Some deviation arising between the predicted and test curves could be attributed to possible bending in the column specimens and other minor alignment issues with the vertical shafts while conducting the experimental investigation. In Fig. 24 (b, d and f), the higher second stiffness than the predicted curve could possibly because of reduction in slip in sleeve due to infill concrete, which was not able to capture by the component model at this stage. To further ensure the applicability of the presented component model to other numerical and experimental tests on hollo bolted CFST connection, few comparison were made with findings from [16, 20] and presented in Fig. 24 (i-l). The plots shows that the component model gives a fair prediction of the numerical and test results. The initial stiffness and the peak load are compared with the experimental and component model prediction values and is presented in Table 8. The average difference of 1% and standard deviation of 6% is achieved for peak load values between component model prediction and experimental values. Whereas the average difference of 4% and standard deviation of 11% is achieved for initial stiffness values between component model prediction and experimental or numerical values.

Thus, the component model presented will be able to predict the global behaviour of the hollo-bolted CFST column connection, with parameters including tube thickness, strength of infill concrete having connection with standard or extended hollo-bolt. Further, the proposed model will also be able to predict the connection behaviour, determining all the three prominent observed failure modes of bolt fracture, column face bending and combined failure.

7 Summary and conclusions

This paper presented the monotonic tensile pull-out tests of single blind-bolted connections to concrete-filled SHS columns. A total of eight specimens were tested, with varying parameters like infill concrete, EHB anchorage length, EHB diameter, steel tube thickness and concrete grade, and the experimental findings are reported here. The research highlights the combined failure modes of the EHB concrete filled SHS connection, which are not reported in existing experiments, and only few numerical and analytical findings were found. A component model for prediction of the bolted connection is presented. The main findings from this paper include:

(a) Three specific failure modes were observed during the experimental programme: column tube-wall bending, bolt fracture, and combined failure of concrete crushing, tube-wall bending and sleeve fracture. In a construction site condition, the combined failure mode would be more appropriate, as this progressive failure of concrete crushing, followed by tube wall deformation and bolt sleeve failure have displayed higher ductility of the connection with sufficient strength and stiffness.

(b) For the failure modes that were dominated by bolt failure, it is confirmed that the location of the shank necking and fracture is between the conical nut and bolt head, and not between conical nut and headed nut. From the bolt strain data, it can also be confirmed that the anchorage element has also been able to significantly improve the connection strength and stiffness. The residual bolt preload for M20 grade 8.8 bolts is about 75%, whereas, for M20 grade 10.9 is about 90%, these factors may also influence the connection behaviour, and should be considered in future FE models.

(c) With a longer bolt anchorage length, the connection capacity has significantly improved, and have led to combined failure mode with concrete strength C25 and C45, and bolt shank failure with C80, suggesting concrete strength as the primary influential factor determining the mode of failures. Therefore, an appropriate strength combination of concrete strength, tube thickness, and anchorage length is required to have combined failure of the connection.

(d) A component model based on non-linear behaviour of individual connection element is presented. Modified equations for predicting strength, stiffness of SHS tube with and without infill concrete under tension have also been presented, which are suitable for hollo bolted connections. The assembly of these models as per spring mechanics gives a good prediction of strength and initial stiffness for such complex connections with an acceptable deviation. This analytical model will be helpful to engineers to identify the failure mode of the connections and make rational design with possible combined failure mode.

Acknowledgement

The authors sincerely acknowledge the support received from the Chinese National Engineering Research Centre for Steel Construction (Hong Kong Branch) at The Hong Kong Polytechnic University.

References:

[1] J. Jiang, J. Zhang, J. Liu, S.P. Chiew, C.K. Lee, Effect of welding and heat treatment on strength of high-strength steel columns, Journal of Constructional Steel Research 151 (2018) 238-252.

[2] J. Chen, T.-M. Chan, A.H. Varma, Stub Column Behavior of Cold-Formed High-Strength Steel Circular Hollow Sections under Compression, Journal of Structural Engineering 146(12) (2020) 04020277.

[3] J.-Y. Zhu, T.-M. Chan, Behaviour of polygonal-shaped steel-tube columns filled with high-strength concrete, Proceedings of the Institution of Civil Engineers - Structures and Buildings 171(2) (2018) 96-112.

[4] A.W. Lacey, W. Chen, H. Hao, K. Bi, Review of bolted inter-module connections in modular steel buildings, Journal of Building Engineering 23 (2019) 207-219.

[5] A.W. Lacey, W. Chen, H. Hao, K. Bi, Structural response of modular buildings – An overview, Journal of Building Engineering 16 (2018) 45-56.

[6] L.-H. Han, W. Li, R. Bjorhovde, Developments and advanced applications of concrete-filled steel tubular (CFST) structures: Members, Journal of Constructional Steel Research 100(C) (2014).

[7] J. Chen, T.-M. Chan, K.-F. Chung, Design of square and rectangular CFST cross-sectional capacities in compression, Journal of Constructional Steel Research 176 (2021) 106419.

[8] W. Li, L.-H. Han, T.-M. Chan, Performance of Concrete-Filled Steel Tubes subjected to Eccentric Tension, Journal of Structural Engineering 141(12) (2015) 04015049.

[9] Lindapter, Brochure of Hollo-Bolt by Lindapter, Bradford, UK, (2018).

[10] AJAX, ONESIDE Brochure B-N012 Data Sheet, (2002).

[11] M. Cabrera, W. Tizani, J. Ninic, A review and analysis of testing and modeling practice of extended Hollo-Bolt blind bolt connections, Journal of Constructional Steel Research 183 (2021) 106763.

[12] H. Agheshlui, H. Goldsworthy, E. Gad, S. Fernando, Tensile behaviour of anchored blind bolts in concrete filled square hollow sections, Materials and Structures 49(4) (2016) 1511-1525.

[13] Y. Oktavianus, H. Yao, H.M. Goldsworthy, E.F. Gad, Pull-out behaviour of blind bolts from concrete-filled tubes, Proceedings of the Institution of Civil Engineers - Structures and Buildings 168(10) (2015) 747-759.

[14] H. Agheshlui, H. Goldsworthy, E. Gad, H. Yao, Tensile Behavior of Groups of Anchored Blind Bolts within Concrete-Filled Steel Square Hollow Sections, Journal of Structural Engineering 142(2) (2016) 04015125.

[15] W. Tizani, D.J. Ridley-Ellis, The performance of a new blind-bolt for moment-resisting connections, Tubular Structures X: Proceedings of the 10th International Symposium on Tubular Structures, Madrid, Spain, 2003, pp. 395-400.

[16] T. Pitrakkos, W. Tizani, Experimental behaviour of a novel anchored blind-bolt in tension, Engineering Structures 49 (2013) 905-919.

[17] P.P. Debnath, T.-M. Chan, Experimental performance of single blind-bolted CFST column connection under predominant shear loading, Journal of Constructional Steel Research 196 (2022) 107386.

[18] W. Tizani, T. Pitrakkos, Performance of T-Stub to CFT Joints Using Blind Bolts with Headed Anchors, Journal of Structural Engineering 141(10) (2015) 04015001.

[19] W. Tizani, M. Mahmood, D. Bournas, Effect of Concrete Infill and Slenderness on Column-Face Component in Anchored Blind-Bolt Connections, Journal of Structural Engineering 146(4) (2020) 04020041.

[20] P.P. Debnath, T.-M. Chan, Tensile behaviour of headed anchored hollo-bolts in concrete filled hollow steel tube connections, Engineering Structures 234 (2021) 111982.

[21] P.P. Debnath, T.-M. Chan, A comprehensive numerical approach for modelling blind-bolted CFST connections, Structures 33 (2021) 2208-2225.
[22] M. Cabrera, W. Tizani, M. Mahmood, M.F. Shamsudin, Analysis of Extended Hollo-Bolt connections: Combined failure in tension, Journal of Constructional Steel Research 165 (2020) 105766.
[23] ISO, British Standards Institution 6892-1:2019(EN)

Metallic materials — Tensile testing — Part 1: Method of test at room temperature, (2019).
[24] M. Cabrera, W. Tizani, J. Ninic, F. Wang, Experimental and numerical analysis of preload in Extended Hollo-Bolt blind bolts, Journal of Constructional Steel Research 186 (2021) 106885.
[25] Y. Oktavianus, H. Chang, H.M. Goldsworthy, E.F. Gad, Component model for pull-out behaviour of headed anchored blind bolt within concrete filled circular hollow section, Engineering Structures 148 (2017) 210-224.
[26] T. Pitrakkos, W. Tizani, A component method model for blind-bolts with headed anchors in tension, Steel and Composite Structures 18(5) (2014) 1305-1330.
[27] AISI, AISI S100-16 North American Specification for the Design of Colf-Formed Steel Structural Members (2016).
[28] Y. Liu, C. Málaga-Chuquitaype, A.Y. Elghazouli, Response and component characterisation of semi-rigid connections to tubular columns under axial loads, Engineering Structures 41 (2012) 510-532.
[29] C. Málaga-Chuquitaype, A.Y. Elghazouli, Component-based mechanical models for blind-bolted angle connections, Engineering Structures 32(10) (2010) 3048-3067.
[30] ACI, Committee 318, Building Code Requirements for Structural Concrete (ACI 318-11) and Commentary (ACI 318R-11), (2011).

[31] Rolf Eligehausen, Rainer Mallée, J.F. Silva, Anchorage in Concrete Construction, John Wiley & Sons2006.

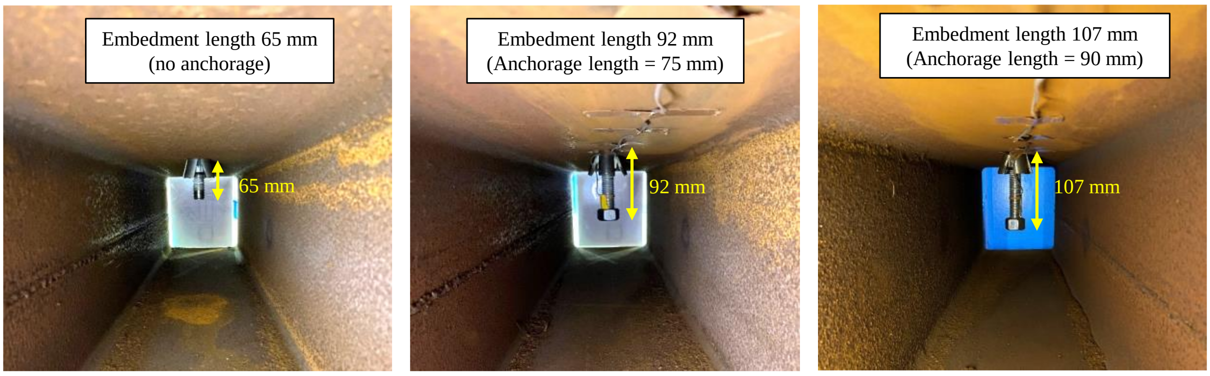

Fig..1: Internal view of steel tube with single hollo-bolted connection with different embedment lengths.

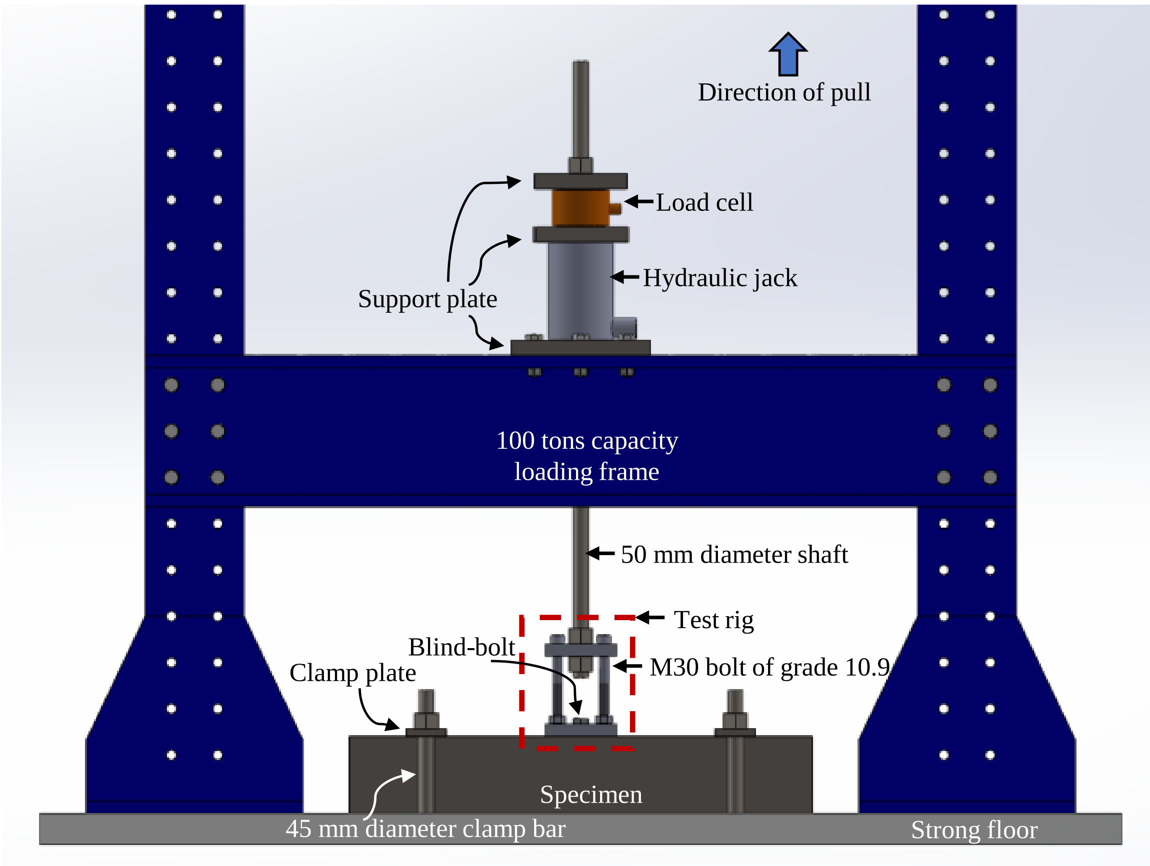

(a)

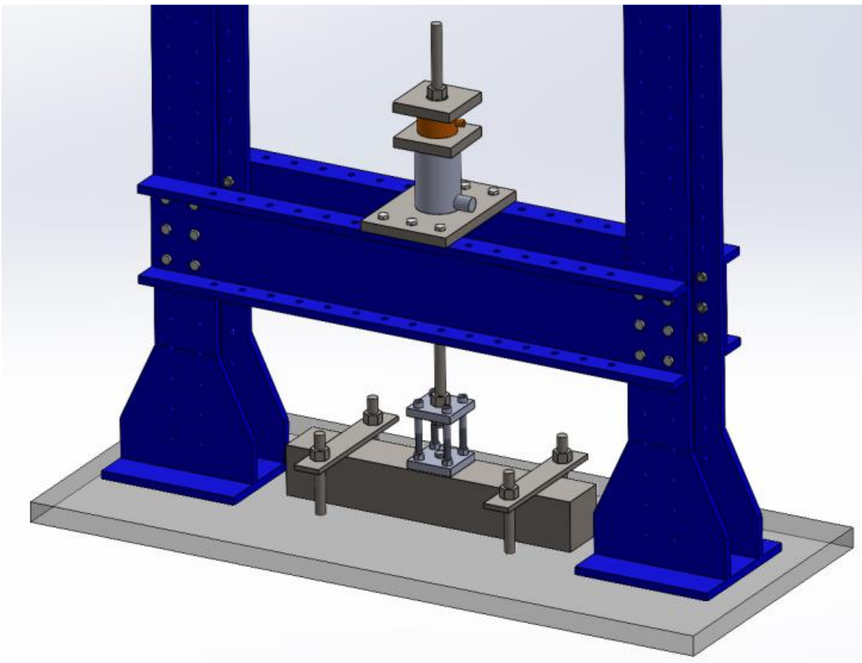

(b)

Fig. 2: (a) Schematic 2D representation of the test set up; (b) 3D view of the test set up.

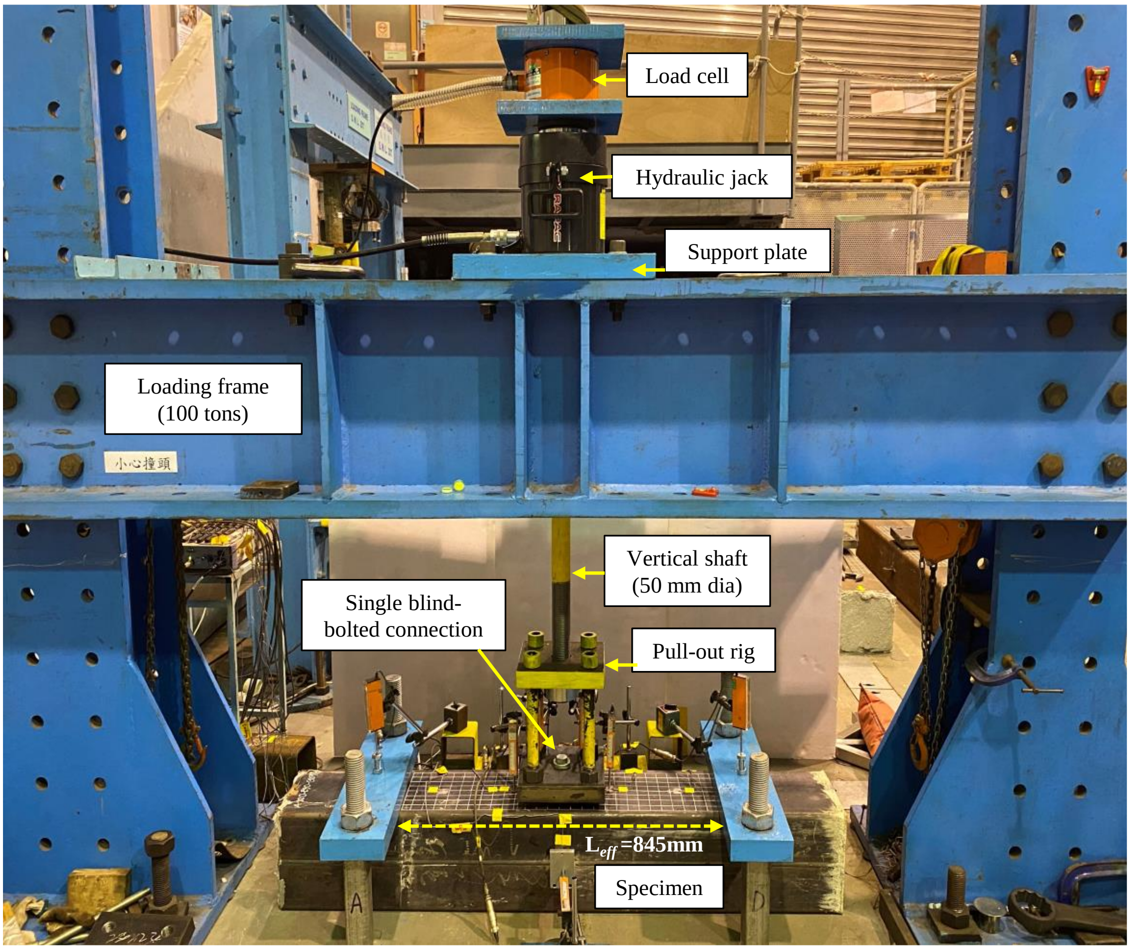

Fig. 3: Experimental setup of CFST with single-bolted connection.

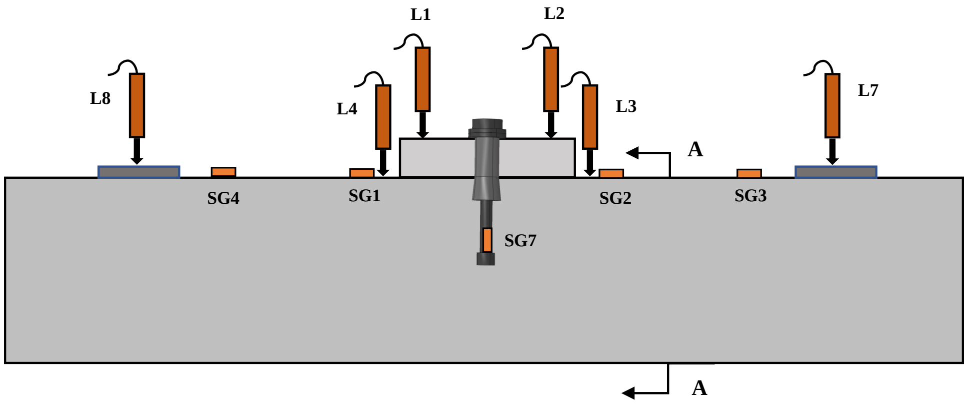

(a) Elevation view for arrangement of instrumentation.

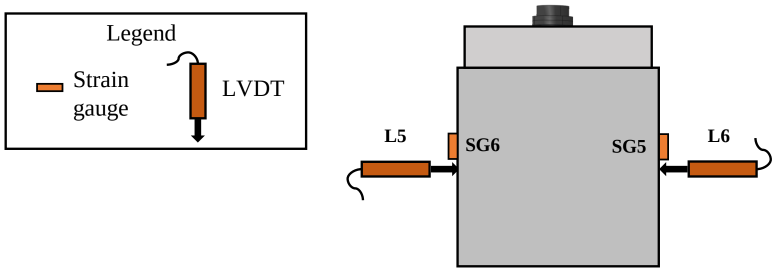

(b) Arrangement of instrumentation at section A-A.

Fig.4: Schematic representation for arrangement of displacement transducer and strain gauges.

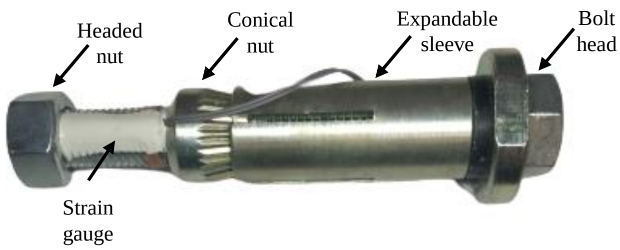

Fig.5: Identification of the parts of extended blind-bolt and positioning of strain gauge.

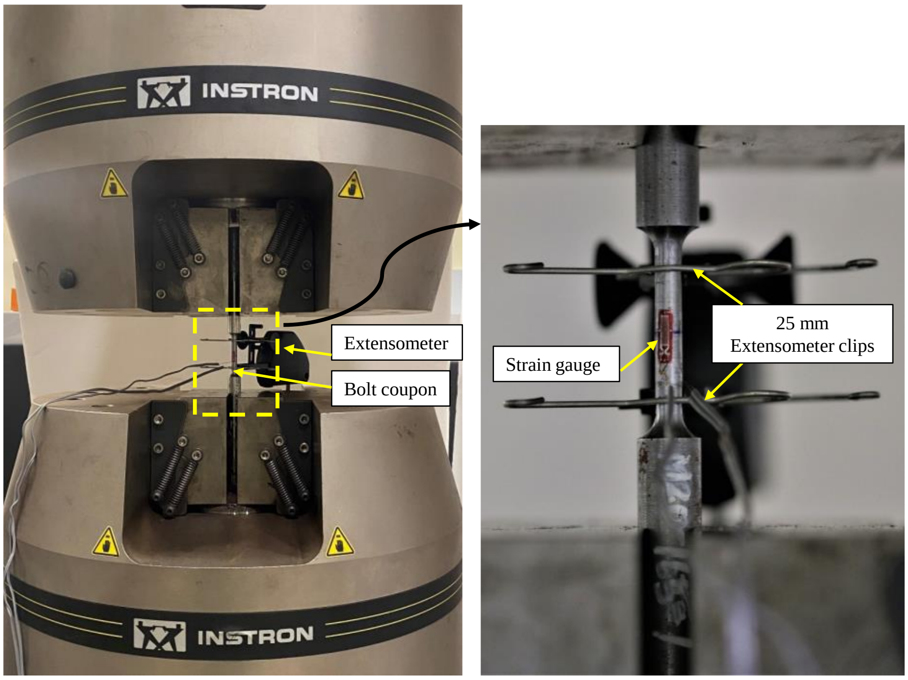

Fig.6: Setup for bolt material test using Instron 8803 servo hydraulic system.

(a) Steel flat coupons (b) Steel curved coupons (c) Bolt circular coupons

Fig.7: Samples of steel flat coupons, curved coupons, and bolt circular coupons after tensile testing.

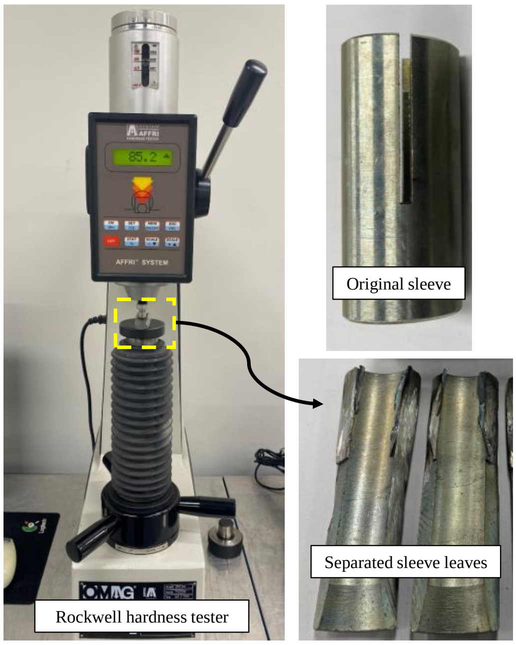

Fig.8: Hardness measurement for bolt sleeve component.

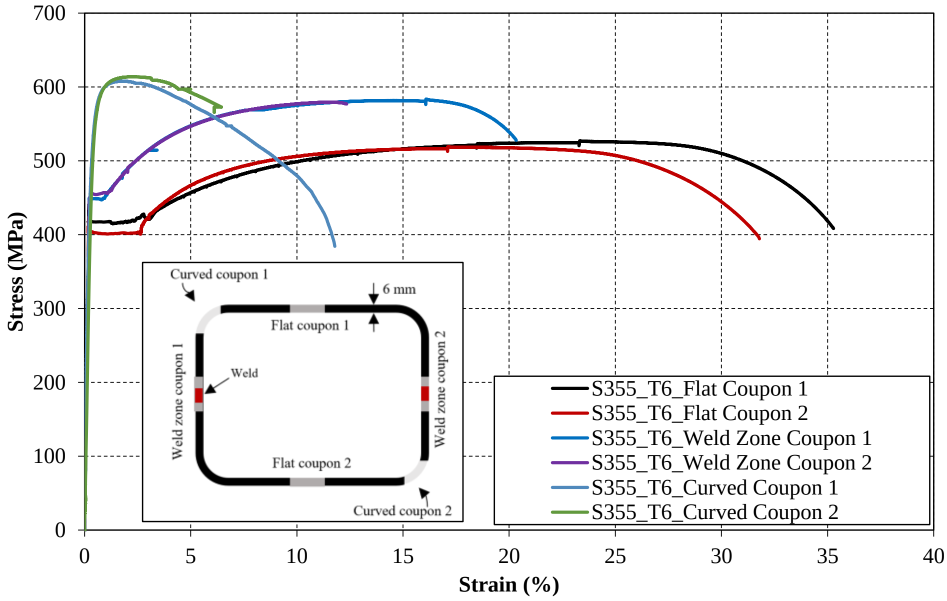

Fig.9: Stress-strain curves for steel tube of thickness 6mm for flat, weld and curve regions.

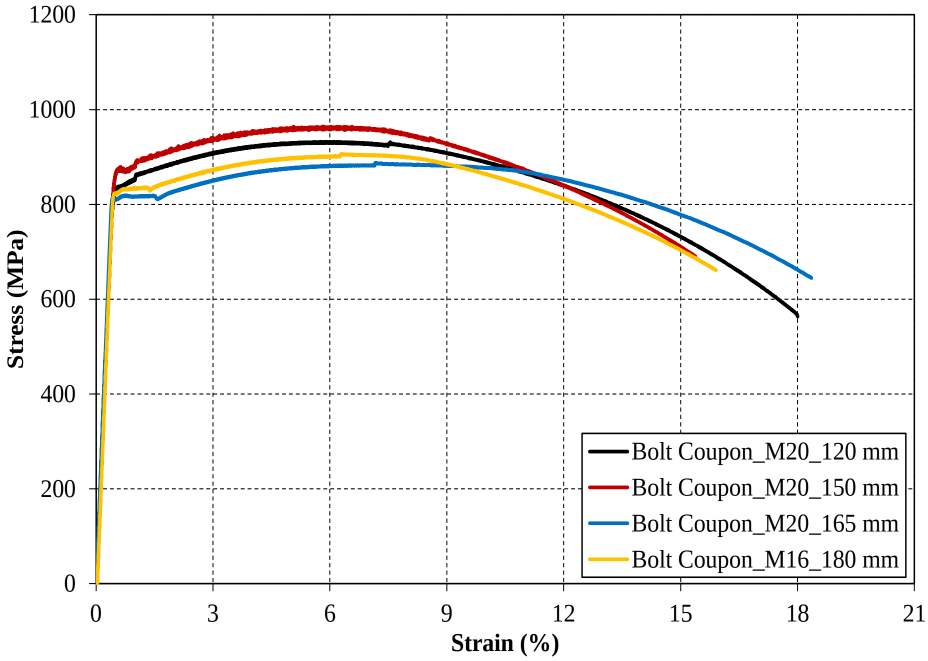

Fig. 10: Stress-strain curves for bolt coupons.

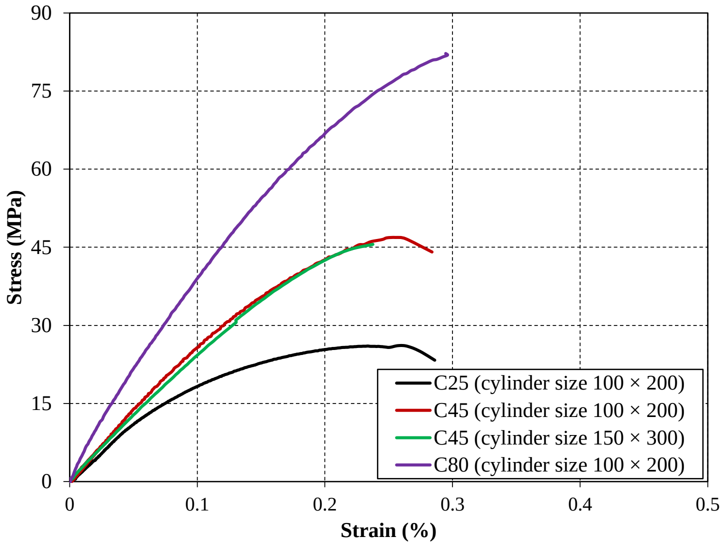

Fig.11: Stress-strain curves for concrete grades C25, C45 and C80.

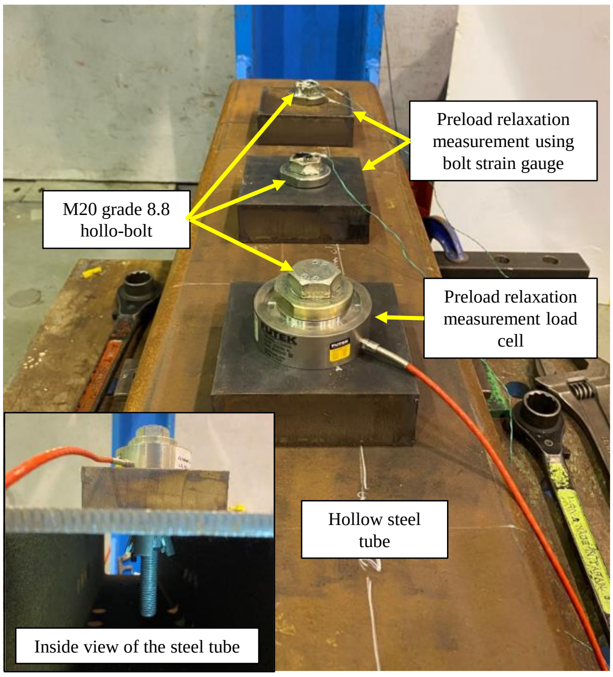

Fig.12: Arrangement for measurement of bolt preload.

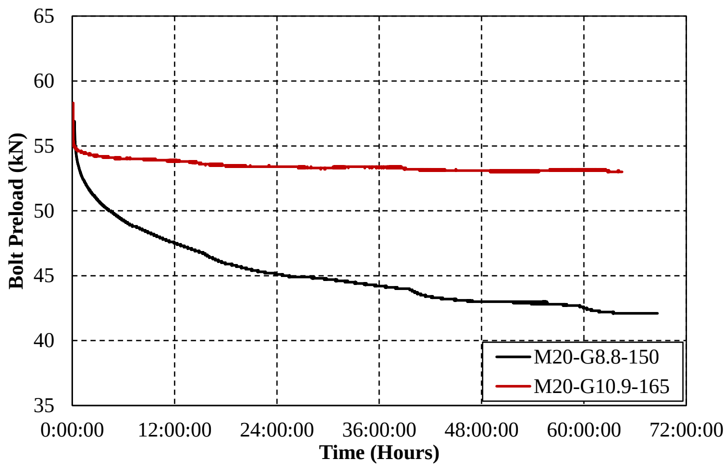

Fig.13: Bolt preload relaxation curves of M20 bolts of two grades.

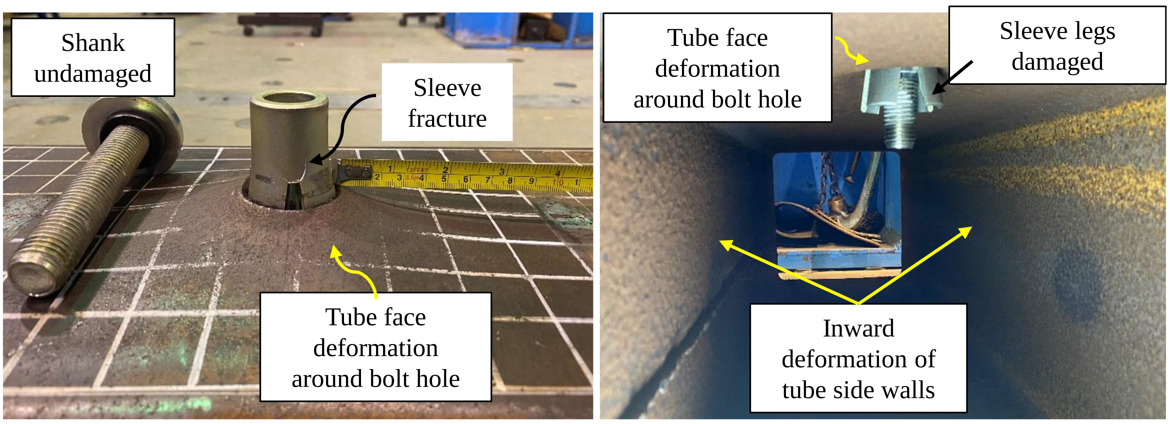

(a) (b)

Fig.14: Specimen A-M20-E0-C0-T8 at failure (a) sleeve fracture and tube face deformation, and (b) tube side wall deformation.

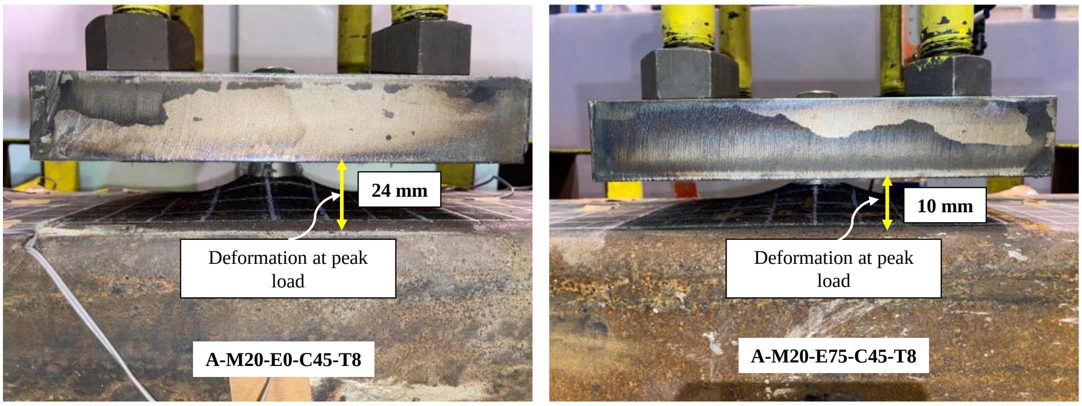

(a) (b)

Fig.15: Deformation at peak loads for specimen (a) A-M20-E0-C45-T8, and (b) A-M20-E75-C45-T8.

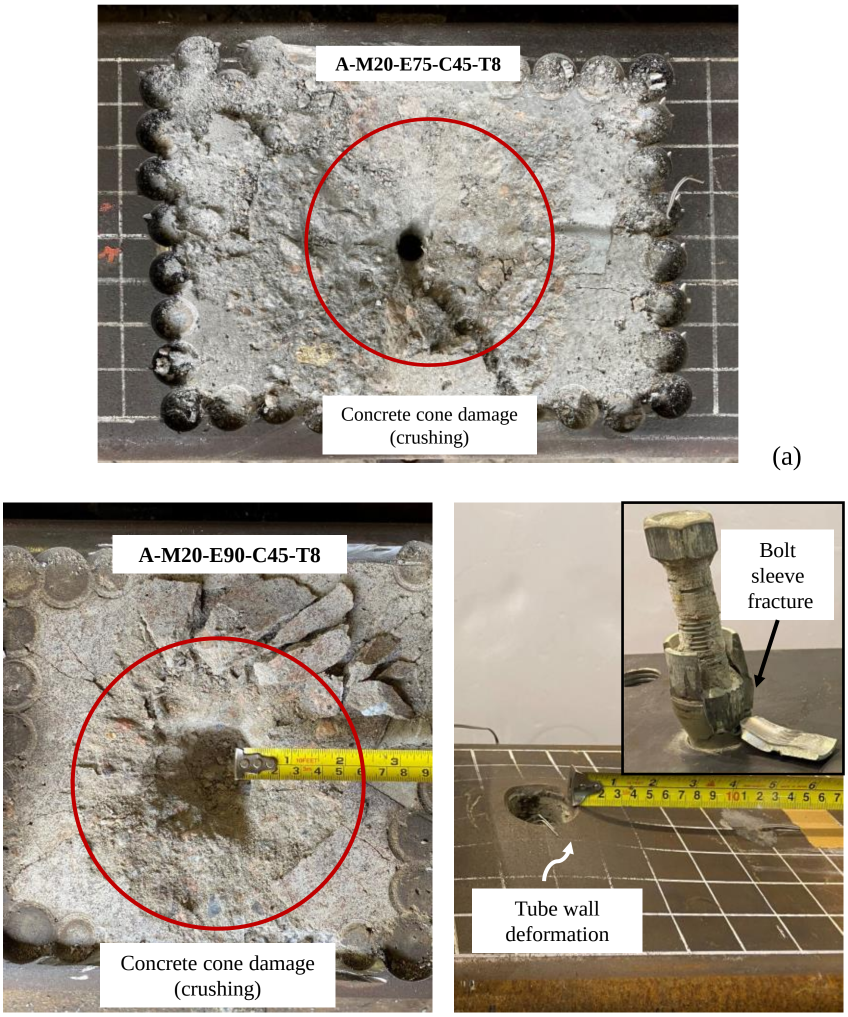

(a) (b)

Fig.16: (a) Concrete cone formation for the specimen A-M20-E75-C45-T8; (b) Concrete cone damage, tube wall deformation and bolt sleeve fracture for the specimen A-M20-E90-C45-T8.

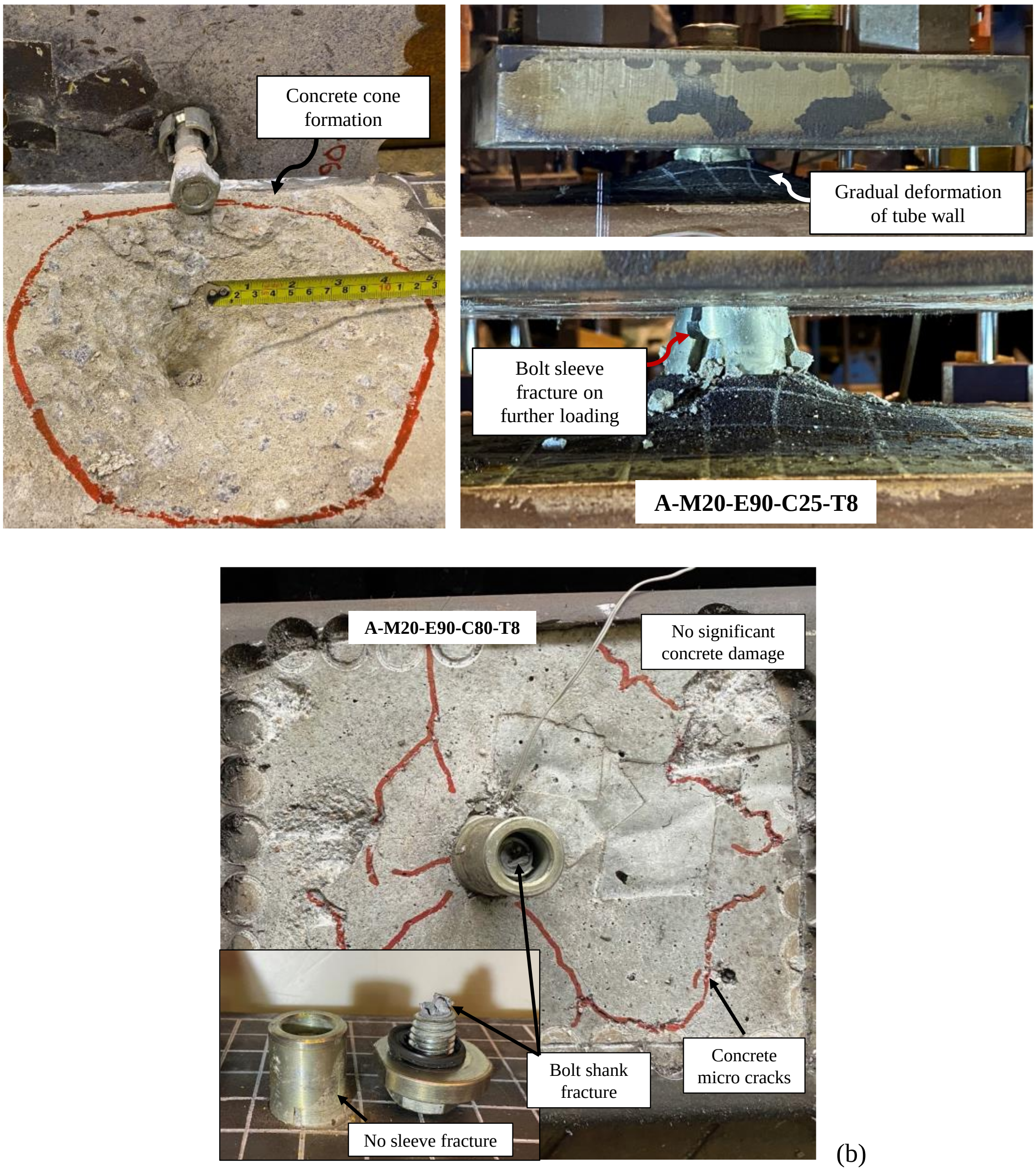

(a)

(b)

Fig.17: (a) Stages of failure: concrete cone failure, deformation of tube wall and bolt sleeve fracture for the specimen A-M20-E90-C25-T8; (b) Limited concrete damage for the specimen A-M20-E90-C80-T8.

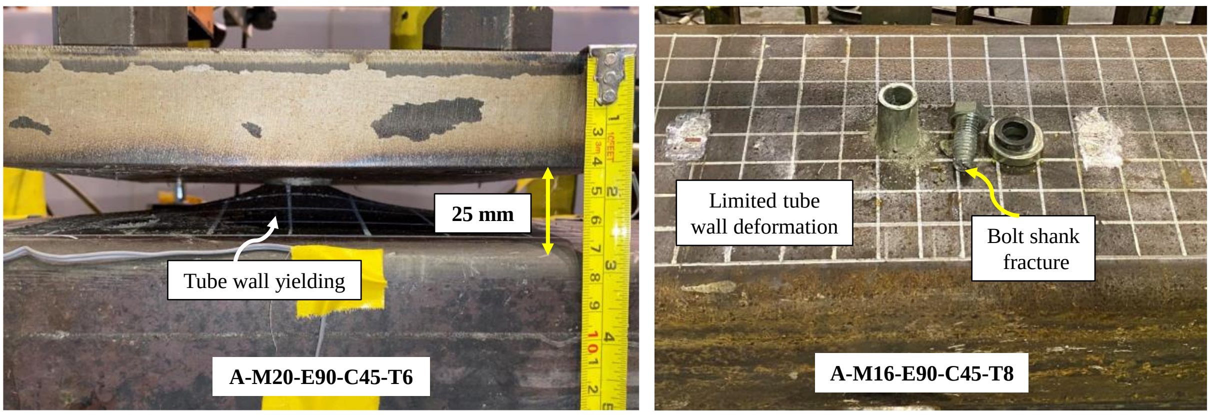

(a) (b)

Fig.18: (a) Tube wall yielding for the specimen A-M20-E90-C45-T6; (b) Bolt shank fracture for the specimen A-M16-E90-C45-T8.

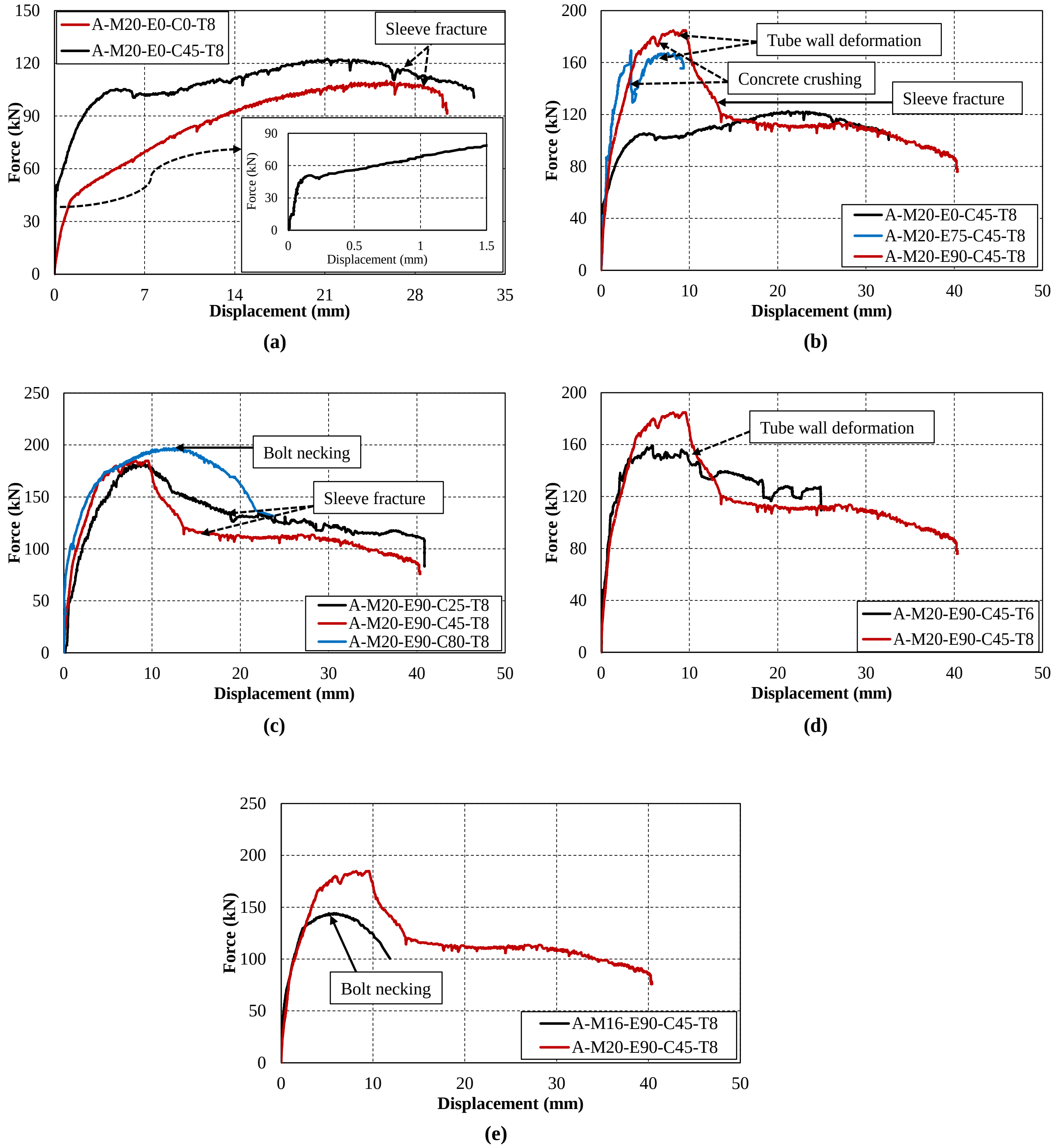

Fig.19: Load-displacement curves.

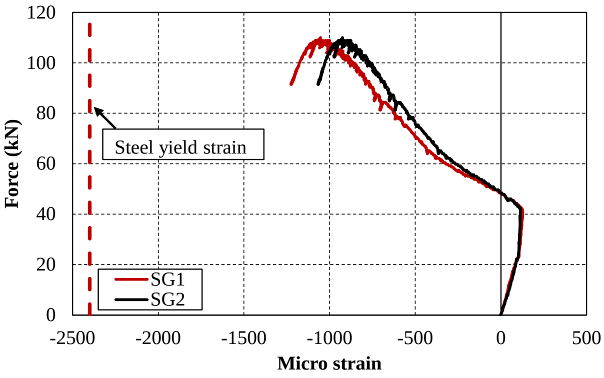

(a) A-M20-E0-C0-T8

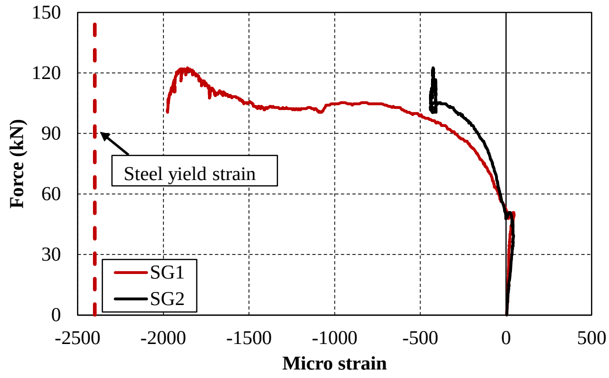

(b) A-M20-E0-C45-T8

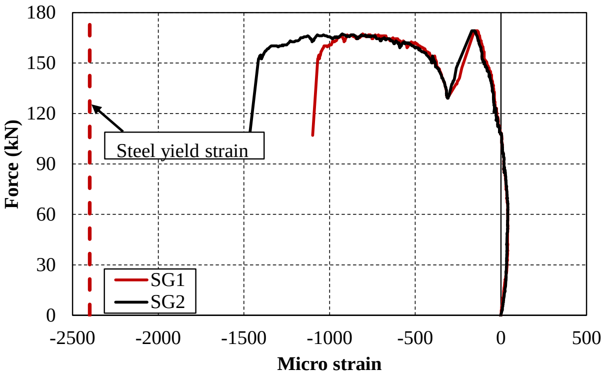

(c) A-M20-E75-C45-T8

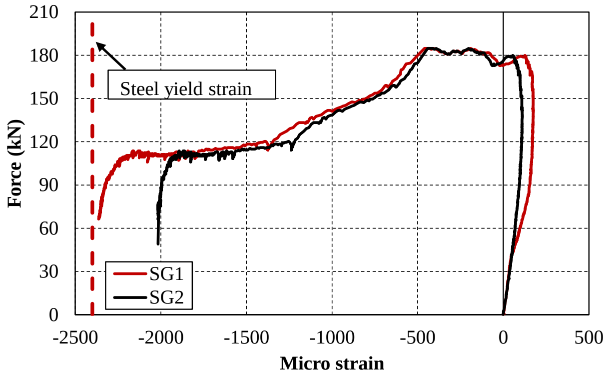

(d) A-M20-E90-C45-T8

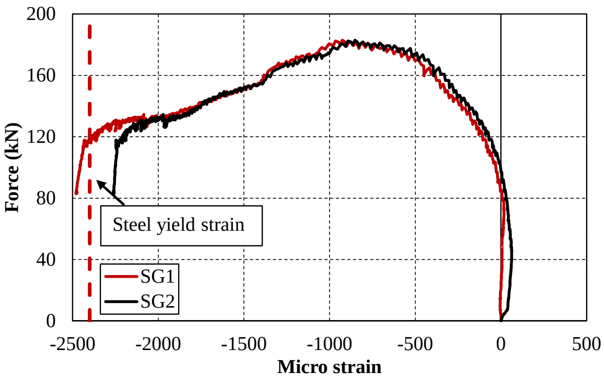

(e) A-M20-E90-C25-T8

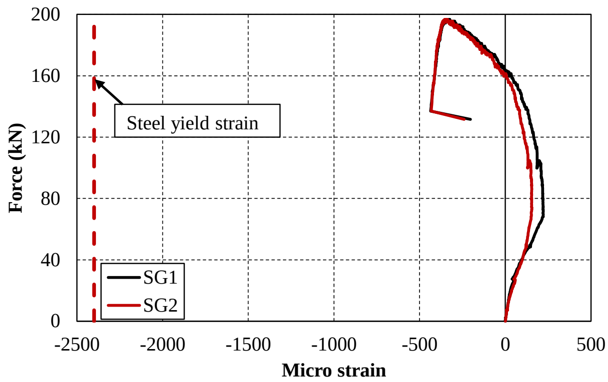

(f) A-M20-E90-C80-T8

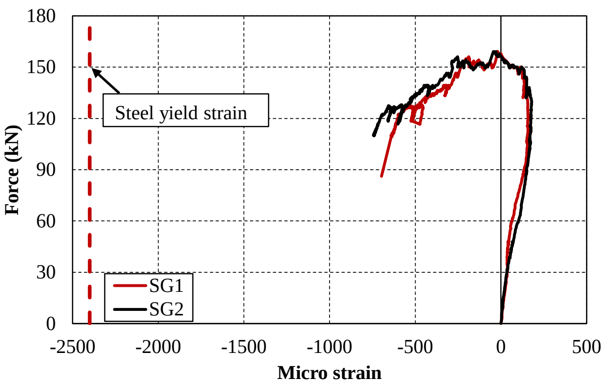

(g) A-M20-E90-C45-T6

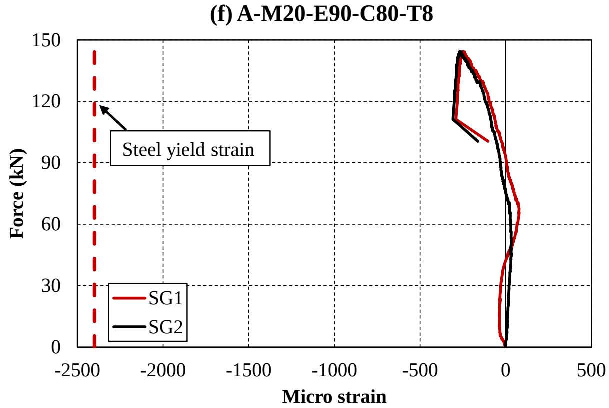

(h) A-M16-E90-C45-T8

Fig.20: Strain developed in steel tube near the connection (SG1 and SG2).

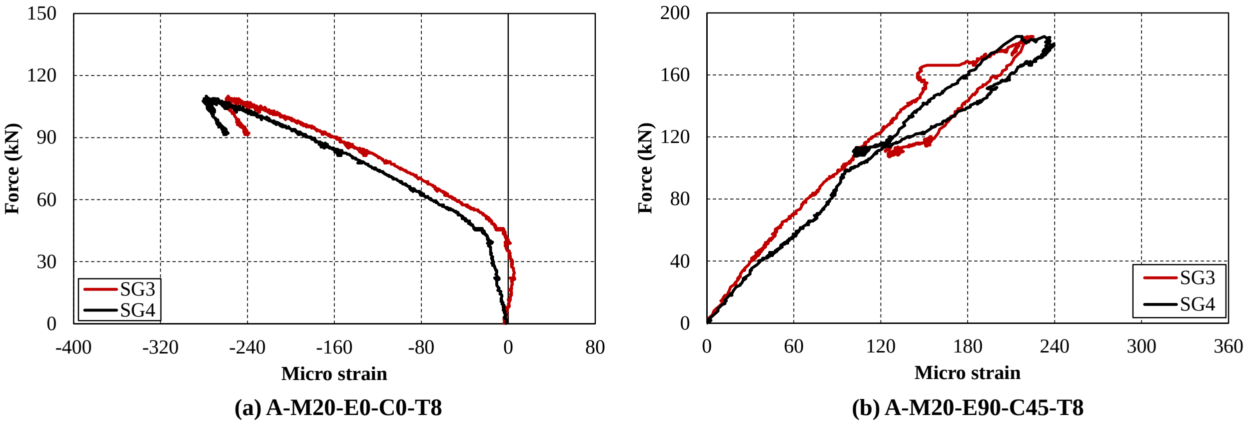

Fig.21: Representative strain developed in steel tube surface between the connection and support (SG3 and SG4).

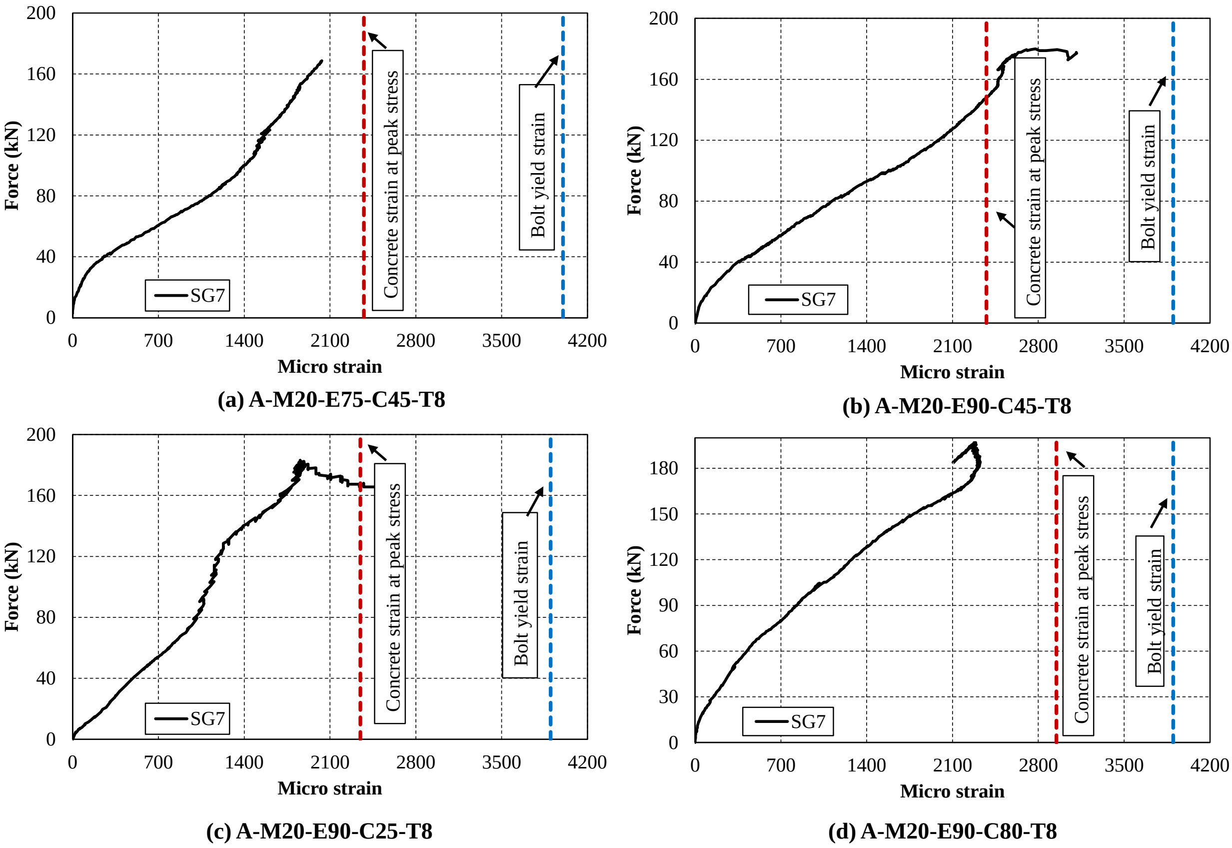

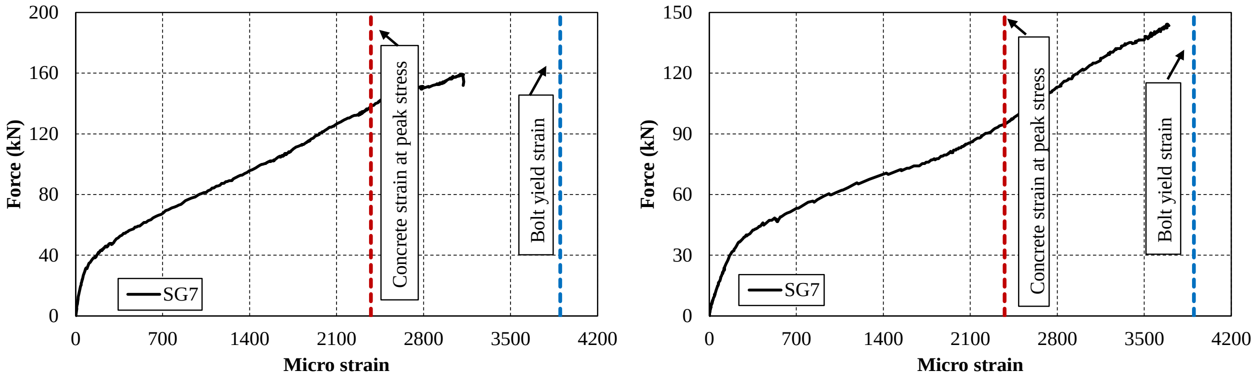

(e) A-M20-E90-C45-T6 **(f) A-M16-E90-C45-T8**

Fig.22: Strain developed at the bolt shank (SG7).

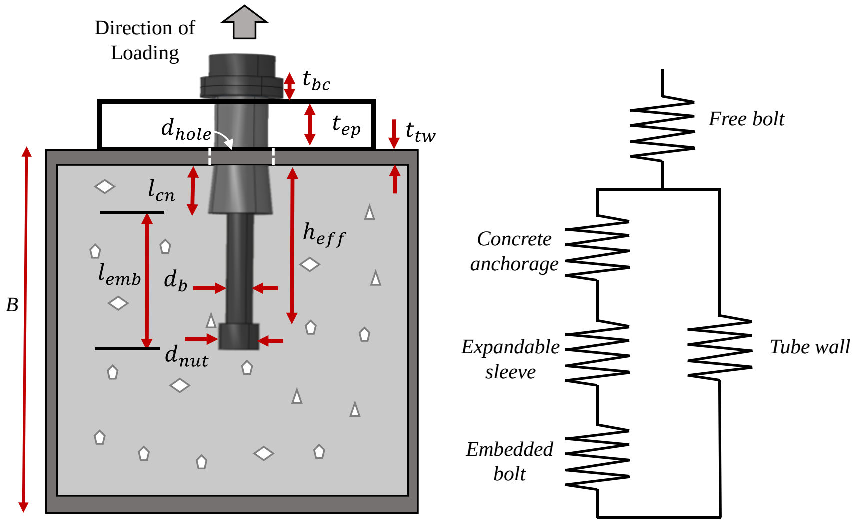

(a) (b)

Fig.23: (a) Identification of connection components; (b) spring assembly.

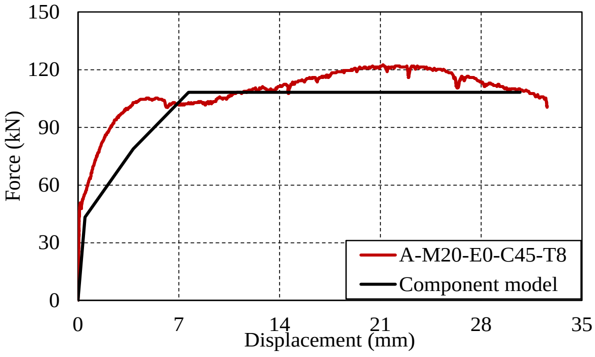
Force (kN)
Displacement (mm)
A-M20-E0-C45-T8
Component model

(a)

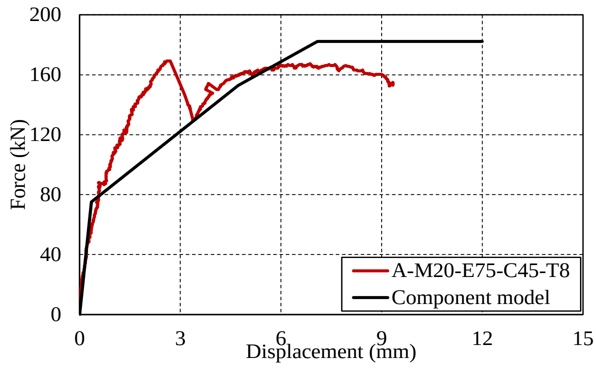
Force (kN)
Displacement (mm)
A-M20-E75-C45-T8
Component model

(b)

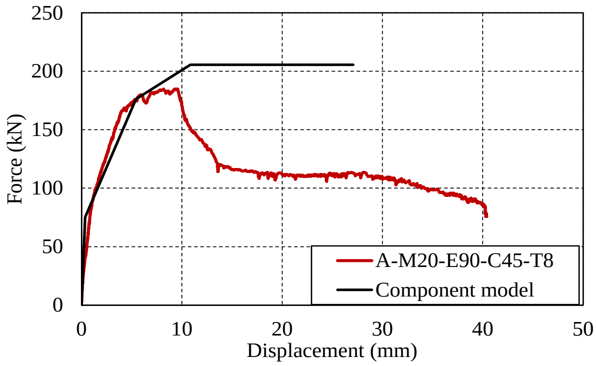
Force (kN)
Displacement (mm)
A-M20-E90-C45-T8
Component model

(c)

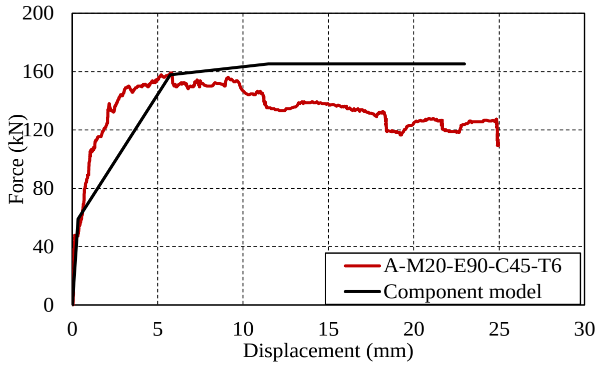
Force (kN)
Displacement (mm)
A-M20-E90-C45-T6
Component model

(d)

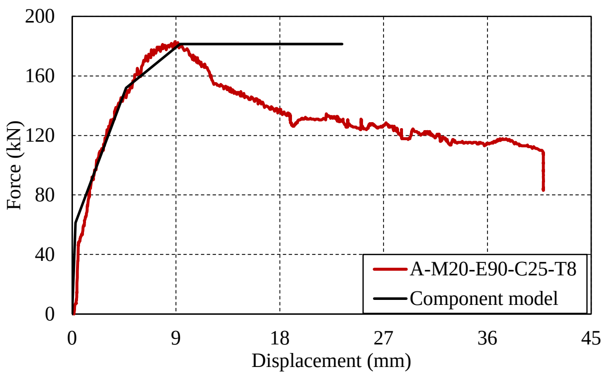
Force (kN)
Displacement (mm)
A-M20-E90-C25-T8
Component model

(e)

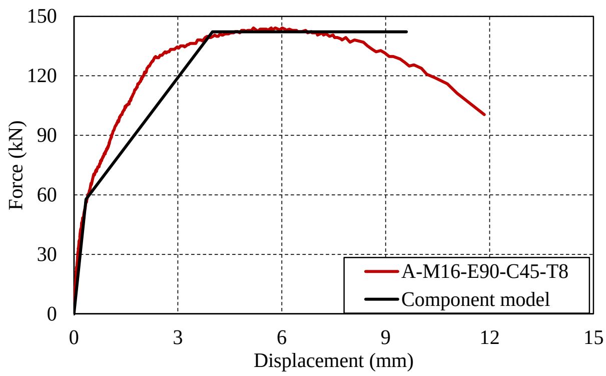
Force (kN)
Displacement (mm)
A-M16-E90-C45-T8
Component model

(f)

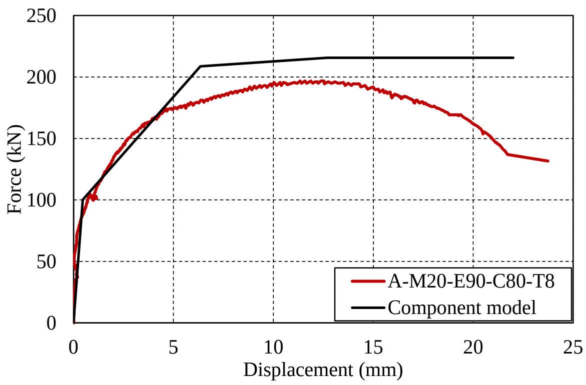
Force (kN)
Displacement (mm)
A-M20-E90-C80-T8
Component model

(g)

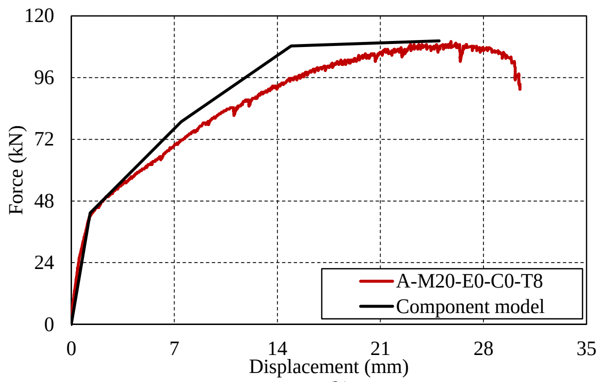
Force (kN)
Displacement (mm)
A-M20-E0-C0-T8
Component model

(h)

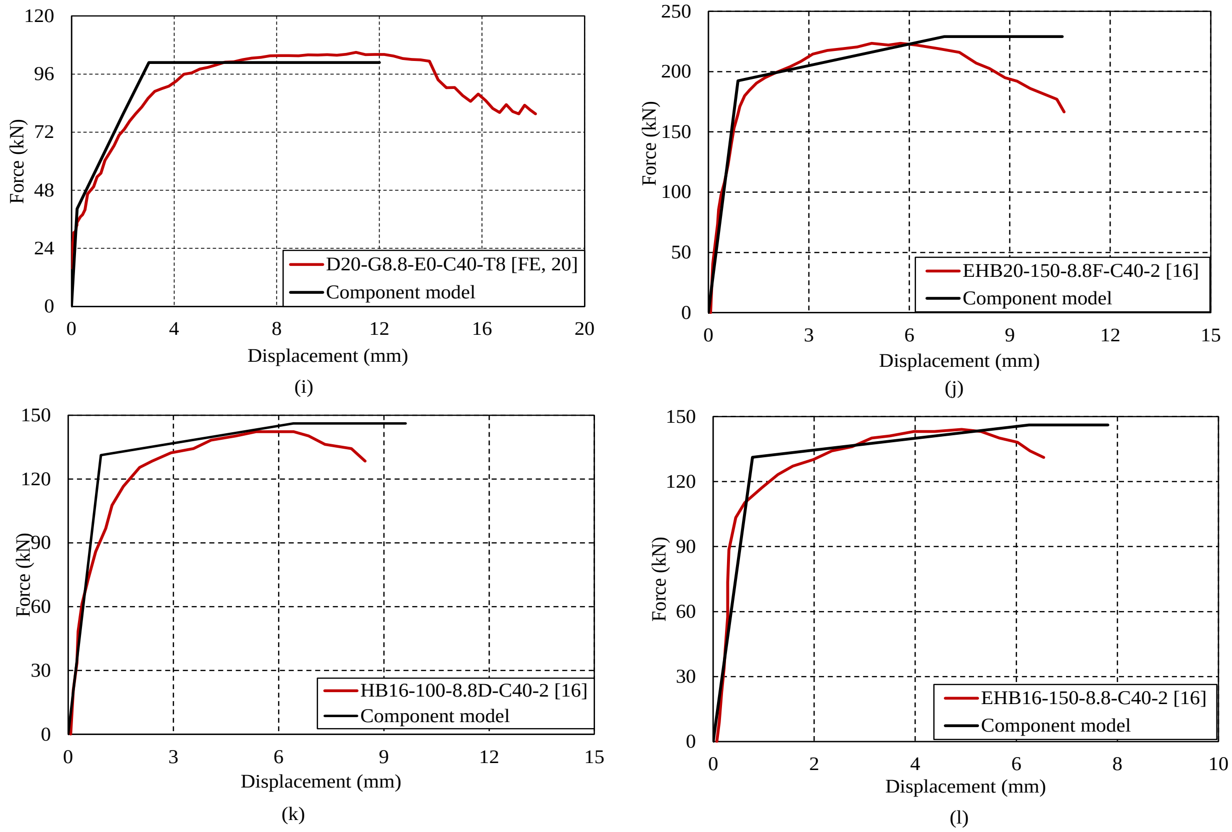

Fig. 24: Validation of global connection behaviour with proposed component model.

Table 1 Geometric dimensions of the specimens.

Specimen ID	Tube length		Column section		b/t	Corner thickness (mm)	Bolt hole location	Bolt hole diameter (mm)
	Actual length (l) (mm)	Effective length (l_{eff}) (mm)	Nominal ($b \times b \times t$) (mm)	Actual ($b \times b \times t$) (mm)				
A-M20-E0-C0-T8	1500	845	250×250×8	251×251.5×8.2	30.6	8.4	Centre	34.7
A-M20-E0-C45-T8	1500	845	250×250×8	250×250.5×8.2	30.4	8.25	Centre	34.8
A-M20-E75-C45-T8	1500	845	250×250×8	250×251×8.2	30.4	8.4	Centre	34.8
A-M20-E90-C45-T8	1500	845	250×250×8	250×249×8.2	30.4	8.42	Centre	34.8
A-M20-E90-C25-T8	1500	845	250×250×8	250×250.5×8.2	30.4	8.42	Centre	34.8
A-M20-E90-C80-T8	1500	845	250×250×8	250×250.5×8.3	30.1	8.45	Centre	34.8
A-M20-E90-C45-T6	1500	845	250×250×8	250×250×8.3	30.1	8.45	Centre	34.7
A-M16-E90-C45-T8	1500	845	250×250×6	248×252×5.9	42	6.0	Centre	28.0

Table 2 Geometric dimensions of the bolts and other information.

Specimen ID	Bolt diameter (mm)	Tensile stress area (mm^2)	Shank length (mm)	Embedment length (mm)	Nut Length (mm)	Anchorage	Anchorage length (mm) (col.5 - col.6)	Bolt torque (Nm)	Bolt grade	Concrete nominal strength
A-M20-E0-C0-T8	19.7	245	120	62	_	No	_	300	8.8	_
A-M20-E0-C45-T8	19.6	245	120	62	_	No	_	300	8.8	45
A-M20-E75-C45-T8	19.7	245	150	92	17	Yes	75	300	8.8	45
A-M20-E90-C45-T8	19.8	245	165	107	17	Yes	90	300	8.8	45
A-M20-E90-C25-T8	19.8	245	165	107	17	Yes	90	300	8.8	25
A-M20-E90-C80-T8	19.8	245	165	107	17	Yes	90	300	8.8	80
A-M20-E90-C45-T6	19.8	245	165	109	17	Yes	92	300	8.8	45
A-M16-E90-C45-T8	15.8	157	165	107	15	Yes	92	190	8.8	45

Table 3 Measured mechanical properties of bolt components and steel tube.

Steel components			f_y (MPa)	f_u (MPa)	E_s (GPa)	f_u/ f_y
Bolt	Shank	Bolt-M20-120 mm	793	934	208	1.17
		Bolt-M20-150 mm	839	967	206	1.15
		Bolt-M20-165 mm	799	887	208	1.11
		Bolt-M16-180 mm	813	906	208	1.11
	Sleeve#	Bolt-M20-120 mm	396	529	_	1.33
		Bolt-M20-150 mm	390	519	_	1.33
		Bolt-M20-165 mm	393	520	_	1.32
		Bolt-M16-180 mm	430	560	_	1.30
Steel tube	Flat region	Nominal thickness 6 mm	411	523	213	1.27
		Nominal thickness 8 mm	352	483	204	1.37
	Curved region	Nominal thickness 6 mm	532	610	214	1.14
		Nominal thickness 8 mm	609	660	200	1.08

Note: #material properties based on Rockwell hardness test.

Table 4 Chemical composition (in %) of M20 blind-bolts as per mill certificates.

Bolt	C	Mn	P	S	Si	Cu	Ni	Cr	Mo	Al	B
M20-120 mm	0.34	0.83	0.17	0.03	0.22	_	_	_	_	0.19	0.19
M20-150 mm	0.34	0.86	0.12	0.06	0.19	0.02	0.01	0.14	_	0.36	0.17
M20-165 mm	0.35	0.78	0.014	0.005	0.21	_	0.10	0.18	0.30	_	0.002

Table 5 Mix design and strength properties of concrete.

Concrete grade	Water/ Cement	Water (Kg/m^3)	Cement (Kg/m^3)	Sand (Kg/m^3)	Aggregate (Kg/m^3)		S.P* (Kg/m^3)	Slump (mm)	Cylinder compressive strength (N/mm^2)	Split tensile strength (N/mm^2)	Elastic modulus E_C (GPa)
					10 mm	20 mm					
C25	0.65	220	340	700	380	760	_	130	26	2.7	23.8
C45	0.48	192	400	720	410	615	2.5	100	46	4.1	25.5
C80	0.28	140	500	704	422	633	10	100	82	6.8	39.6

Note: S.P* refers to superplasticizer.

Table 6 Bolt preload test details.

Bolt ID	Diameter (mm)	Property class	Shank length (mm)	Torque (Nm)	$F_{p,ini}$ (kN)	$F_{p,48\,h}$ (kN)	$F_{p,48\,h}$ / $F_{p,ini}$
M20-G8.8-150	20	8.8	150	300	56	43	0.76
M20-G8.8-165	20	8.8	165	300	56	44	0.78
M20-G10.9-165	20	10.9	165	340	58	53	0.91

$F_{p,ini}$ refers to initial preload; $F_{p,48\,h}$ refers to residual preload after 48 h.

Table 7 Measured stiffness, capacities, and deformation of the connections.

Specimen	Test peak load (kN)	Bolt ultimate capacity (kN)	Deformation at peak load (mm)	Stiffness at 50% bolt capacity (kN/mm)	Failure mode
A-M20-E0-C0-T8	110	228	25.8	4.26	Column wall deformation
A-M20-E0-C45-T8	123	228	21.2	7.46	Column wall deformation
A-M20-E75-C45-T8	170	237	2.6	82.5	Concrete crushing-column wall deformation
A-M20-E90-C45-T8	185	217	9.27	75.1	Concrete crushing-column wall deformation-partial bolt failure
A-M20-E90-C25-T8	183	217	6.5	63.2	Concrete crushing-column wall deformation-partial bolt failure
A-M20-E90-C80-T8	197	217	12.4	95.9	Bolt failure
A-M20-E90-C45-T6	159	217	4.7	97.7	Concrete crushing-column wall deformation
A-M16-E90-C45-T8	144	142	5.2	111.2	Bolt failure

Table 8 Comparison of component model with experimental and FE results.

Specimen	Initial stiffness (Experiment or FEA) $K_{Exp/FEA}$ (kN/mm)	Peak load (Experiment or FEA) $P_{Exp/FEA}$ (kN)	Initial stiffness (Component model) K_{Comp} (kN/mm)	Peak load (Component model) P_{Comp} (kN)	$\frac{P_{Comp}}{P_{Exp\ or\ FEA}}$	$\frac{K_{Comp}}{K_{Exp\ or\ FEA}}$
A-M20-E0-C0-T8	32.1	110	28.5	109	0.99	0.88
A-M20-E0-C45-T8	89	123	70	108	0.87	0.78
A-M20-E75-C45-T8	157.5	170	173.2	182	1.07	1.09
A-M20-E90-C45-T8	177.7	185	174.4	205	1.10	0.98
A-M20-E90-C25-T8	125	183	151	181	0.98	1.19
A-M20-E90-C80-T8	173.3	197	178	215	1.09	1.02
A-M20-E90-C45-T6	156	159	143	165	1.03	0.91
A-M16-E90-C45-T8	140	144	134	142	0.98	0.95
D20-G8.8-E0-C40-T8 [FE, 20]	127	105	117	101	0.96	0.92
EHB20-150-8.8F-C40-2 [16]	182	227	176	229	1.00	0.96
HB16-100-8.8D-C40-2 [16]	89	142	97	146	1.02	1.08
EHB16-150-8.8D-C40-2 [16]	165	144	136	146	1.01	0.82
				Mean	*1.01*	*0.96*
				Standard deviation	*0.06*	*0.11*